Four-jet final state production in e^+e^- collisions at center-of-mass energies of 130 and 136 GeV

D. Buskulic, I. De Bonis, D. Decamp, P. Ghez, C. Goy, J.P. Lees, A. Lucotte,
M.N. Minard, P. Odier, B. Pietrzyk, et al.

▶ To cite this version:

HAL Id: in2p3-00001272
http://hal.in2p3.fr/in2p3-00001272

Submitted on 1 Apr 1999

Four-jet final state production in e⁺e⁻ collisions at centre-of-mass energies of 130 and 136 GeV

The ALEPH Collaboration*)

Abstract

The four-jet final state is analyzed to search for hadronic decays of pair-produced heavy particles. The analysis uses the ALEPH data collected at LEP in November 1995 at centre-of-mass energies of 130 and 136 GeV, corresponding to a total integrated luminosity of 5.7 pb^{-1}. An excess of four-jet events is observed with respect to the standard model predictions. In addition, these events exhibit an enhancement in the sum of the two di-jet masses around 105 GeV/c^2. The properties of these events are studied and compared to the expectations from standard processes and to pair production hypotheses.

_____

*) See next pages for the list of authors

The ALEPH Collaboration

D. Buskulic, I. De Bonis, D. Decamp, P. Ghez, C. Goy, J.-P. Lees, A. Lucotte, M.-N. Minard, P. Odier, B. Pietrzyk
> Laboratoire de Physique des Particules (LAPP), IN^{2}P^3-CNRS, 74019 Annecy-le-Vieux Cedex, France

M.P. Casado, M. Chmeissani, J.M. Crespo, M. Delfino,[12] I. Efthymiopoulos,[20] E. Fernandez, M. Fernandez-Bosman, Ll. Garrido,[15] A. Juste, M. Martinez, S. Orteu, C. Padilla, A. Pascual, J.A. Perlas, I. Riu, F. Sanchez, F. Teubert
> Institut de Fisica d'Altes Energies, Universitat Autonoma de Barcelona, 08193 Bellaterra (Barcelona), Spain[7]

A. Colaleo, D. Creanza, M. de Palma, G. Gelao, M. Girone, G. Iaselli, G. Maggi,[3] M. Maggi, N. Marinelli, S. Nuzzo, A. Ranieri, G. Raso, F. Ruggieri, G. Selvaggi, L. Silvestris, P. Tempesta, G. Zito
> Dipartimento di Fisica, INFN Sezione di Bari, 70126 Bari, Italy

X. Huang, J. Lin, Q. Ouyang, T. Wang, Y. Xie, R. Xu, S. Xue, J. Zhang, L. Zhang, W. Zhao
> Institute of High-Energy Physics, Academia Sinica, Beijing, The People's Republic of China[8]

R. Alemany, A.O. Bazarko, M. Cattaneo, P. Comas, P. Coyle, H. Drevermann, R.W. Forty, M. Frank, R. Hagelberg, J. Harvey, P. Janot, B. Jost, E. Kneringer, J. Knobloch, I. Lehraus, G. Lutters, E.B. Martin, P. Mato, A. Minten, R. Miquel, Ll.M. Mir,[2] L. Moneta, T. Oest,[1] A. Pacheco, J.-F. Pusztaszeri, F. Ranjard, P. Rensing,[25] L. Rolandi, D. Schlatter, M. Schmelling,[24] O. Schneider, W. Tejessy, I.R. Tomalin, A. Venturi, H. Wachsmuth, A. Wagner
> European Laboratory for Particle Physics (CERN), 1211 Geneva 23, Switzerland

Z. Ajaltouni, A. Barrès, C. Boyer, A. Falvard, P. Gay, C . Guicheney, P. Henrard, J. Jousset, B. Michel, S. Monteil, J-C. Montret, D. Pallin, P. Perret, F. Podlyski, J. Proriol, P. Rosnet, J.-M. Rossignol
> Laboratoire de Physique Corpusculaire, Université Blaise Pascal, IN^{2}P^3-CNRS, Clermont-Ferrand, 63177 Aubière, France

T. Fearnley, J.B. Hansen, J.D. Hansen, J.R. Hansen, P.H. Hansen, B.S. Nilsson, A. Wäänänen
> Niels Bohr Institute, 2100 Copenhagen, Denmark[9]

A. Kyriakis, C. Markou, E. Simopoulou, I. Siotis, A. Vayaki, K. Zachariadou
> Nuclear Research Center Demokritos (NRCD), Athens, Greece

A. Blondel, J.C. Brient, A. Rougé, M. Rumpf, A. Valassi,[6] H. Videau[21]
> Laboratoire de Physique Nucléaire et des Hautes Energies, Ecole Polytechnique, IN^{2}P^3-CNRS, 91128 Palaiseau Cedex, France

E. Focardi,[21] G. Parrini
> Dipartimento di Fisica, Università di Firenze, INFN Sezione di Firenze, 50125 Firenze, Italy

M. Corden, C. Georgiopoulos, D.E. Jaffe
> Supercomputer Computations Research Institute, Florida State University, Tallahassee, FL 32306-4052, USA [13,14]

A. Antonelli, G. Bencivenni, G. Bologna,[4] F. Bossi, P. Campana, G. Capon, D. Casper, V. Chiarella, G. Felici, P. Laurelli, G. Mannocchi,[5] F. Murtas, G.P. Murtas, L. Passalacqua, M. Pepe-Altarelli
> Laboratori Nazionali dell'INFN (LNF-INFN), 00044 Frascati, Italy

L. Curtis, S.J. Dorris, A.W. Halley, I.G. Knowles, J.G. Lynch, V. O'Shea, C. Raine, P. Reeves, J.M. Scarr,

K. Smith, A.S. Thompson, F. Thomson, S. Thorn, R.M. Turnbull

Department of Physics and Astronomy, University of Glasgow, Glasgow G12 8QQ,United Kingdom[10]

U. Becker, C. Geweniger, G. Graefe, P. Hanke, G. Hansper, V. Hepp, E.E. Kluge, A. Putzer, B. Rensch, M. Schmidt, J. Sommer, H. Stenzel, K. Tittel, S. Werner, M. Wunsch

Institut für Hochenergiephysik, Universität Heidelberg, 69120 Heidelberg, Fed. Rep. of Germany[16]

D. Abbaneo, R. Beuselinck, D.M. Binnie, W. Cameron, P.J. Dornan, A. Moutoussi, J. Nash, J.K. Sedgbeer, A.M. Stacey, M.D. Williams

Department of Physics, Imperial College, London SW7 2BZ, United Kingdom[10]

G. Dissertori, P. Girtler, D. Kuhn, G. Rudolph

Institut für Experimentalphysik, Universität Innsbruck, 6020 Innsbruck, Austria[18]

A.P. Betteridge, C.K. Bowdery, P. Colrain, G. Crawford, A.J. Finch, F. Foster, G. Hughes, T. Sloan, E.P. Whelan, M.I. Williams

Department of Physics, University of Lancaster, Lancaster LA1 4YB, United Kingdom[10]

A. Galla, A.M. Greene, C. Hoffmann, K. Kleinknecht, G. Quast, B. Renk, E. Rohne, H.-G. Sander, P. van Gemmeren C. Zeitnitz

Institut für Physik, Universität Mainz, 55099 Mainz, Fed. Rep. of Germany[16]

J.J. Aubert,[21] A.M. Bencheikh, C. Benchouk, A. Bonissent,[21] G. Bujosa, D. Calvet, J. Carr, C. Diaconu, N. Konstantinidis, P. Payre, D. Rousseau, M. Talby, A. Sadouki, M. Thulasidas, A. Tilquin, K. Trabelsi

Centre de Physique des Particules, Faculté des Sciences de Luminy, IN^2P^3-CNRS, 13288 Marseille, France

M. Aleppo, F. Ragusa[21]

Dipartimento di Fisica, Universitá di Milano e INFN Sezione di Milano, 20133 Milano, Italy.

I. Abt, R. Assmann, C. Bauer, W. Blum, H. Dietl, F. Dydak,[21] G. Ganis, C. Gotzhein, K. Jakobs, H. Kroha, G. Lütjens, G. Lutz, W. Männer, H.-G. Moser, R. Richter, A. Rosado-Schlosser, S. Schael, R. Settles, H. Seywerd, R. St. Denis, W. Wiedenmann, G. Wolf

Max-Planck-Institut für Physik, Werner-Heisenberg-Institut, 80805 München, Fed. Rep. of Germany[16]

J. Boucrot, O. Callot, A. Cordier, M. Davier, L. Duflot, J.-F. Grivaz, Ph. Heusse, A. Höcker, M. Jacquet, D.W. Kim,[19] F. Le Diberder, J. Lefrançois, A.-M. Lutz, I. Nikolic, H.J. Park,[19] I.C. Park,[19] M.-H. Schune, S. Simion, J.-J. Veillet, I. Videau, D. Zerwas

Laboratoire de l'Accélérateur Linéaire, Université de Paris-Sud, IN^2P^3-CNRS, 91405 Orsay Cedex, France

P. Azzurri, G. Bagliesi, G. Batignani, S. Bettarini, C. Bozzi, G. Calderini, M. Carpinelli, M.A. Ciocci, V. Ciulli, R. Dell'Orso, R. Fantechi, I. Ferrante, A. Giassi, A. Gregorio, F. Ligabue, A. Lusiani, P.S. Marrocchesi, A. Messineo, F. Palla, G. Rizzo, G. Sanguinetti, A. Sciabà, P. Spagnolo, J. Steinberger, R. Tenchini, G. Tonelli,[26] C. Vannini, P.G. Verdini, J. Walsh

Dipartimento di Fisica dell'Università, INFN Sezione di Pisa, e Scuola Normale Superiore, 56010 Pisa, Italy

G.A. Blair, L.M. Bryant, F. Cerutti, J.T. Chambers, Y. Gao, M.G. Green, T. Medcalf, P. Perrodo, J.A. Strong, J.H. von Wimmersperg-Toeller

Department of Physics, Royal Holloway & Bedford New College, University of London, Surrey TW20 OEX, United Kingdom[10]

D.R. Botterill, R.W. Clifft, T.R. Edgecock, S. Haywood, P. Maley, P.R. Norton, J.C. Thompson, A.E. Wright

Particle Physics Dept., Rutherford Appleton Laboratory, Chilton, Didcot, Oxon OX11 OQX, United Kingdom[10]

B. Bloch-Devaux, P. Colas, S. Emery, W. Kozanecki, E. Lançon, M.C. Lemaire, E. Locci, B. Marx, P. Perez, J. Rander, J.-F. Renardy, A. Roussarie, J.-P. Schuller, J. Schwindling, A. Trabelsi, B. Vallage

CEA, DAPNIA/Service de Physique des Particules, CE-Saclay, 91191 Gif-sur-Yvette Cedex, France[17]

S.N. Black, J.H. Dann, R.P. Johnson, H.Y. Kim, A.M. Litke, M.A. McNeil, G. Taylor

Institute for Particle Physics, University of California at Santa Cruz, Santa Cruz, CA 95064, USA[22]

C.N. Booth, R. Boswell, C.A.J. Brew, S. Cartwright, F. Combley, A. Koksal, M. Letho, W.M. Newton, J. Reeve, L.F. Thompson

Department of Physics, University of Sheffield, Sheffield S3 7RH, United Kingdom[10]

A. Böhrer, S. Brandt, V. Büscher, G. Cowan, C. Grupen, P. Saraiva, L. Smolik, F. Stephan,

Fachbereich Physik, Universität Siegen, 57068 Siegen, Fed. Rep. of Germany[16]

M. Apollonio, L. Bosisio, R. Della Marina, G. Giannini, B. Gobbo, G. Musolino

Dipartimento di Fisica, Università di Trieste e INFN Sezione di Trieste, 34127 Trieste, Italy

J. Putz, J. Rothberg, S. Wasserbaech, R.W. Williams

Experimental Elementary Particle Physics, University of Washington, WA 98195 Seattle, U.S.A.

S.R. Armstrong, L. Bellantoni,[23] P. Elmer, Z. Feng,[28] D.P.S. Ferguson, Y.S. Gao,[29] S. González, J. Grahl, T.C. Greening, O.J. Hayes, H. Hu, P.A. McNamara III, J.M. Nachtman, W. Orejudos, Y.B. Pan, Y. Saadi, M. Schmitt, I.J. Scott, A.M. Walsh,[27] Sau Lan Wu, X. Wu, J.M. Yamartino, M. Zheng, G. Zobernig

Department of Physics, University of Wisconsin, Madison, WI 53706, USA[11]

1   Introduction

The data recorded by the ALEPH detector in November 1995 at centre-of-mass energies of 130 and 136 GeV, are analyzed in the four-jet topology to search for pair-produced heavy particles decaying hadronically. The data sample corresponds to a total integrated luminosity of 5.7 pb^{-1}, equally distributed between 130 and 136 GeV. The analysis described in this article was originally motivated by a search for the $e^+e^- \rightarrow hA \rightarrow b\bar{b}b\bar{b}$ process, but it can also be applied to search for other pair-produced particles such as charged Higgs bosons decaying into $c\bar{s}\bar{c}s$, excited quarks decaying into quark-gluon pairs, or supersymmetric particles with subsequent R-parity violating decays.

The paper is organized as follows. After a short description of the detector in Section 2, the selection of the four-jet topology is detailed in Section 3. The distribution of the sum of the di-jet masses is studied and confronted with the expectation from standard processes. In Section 4, the parton dynamics and the charges of the jets are examined and compared to the standard model predictions. Finally, in Section 5, the properties of these events are interpreted in the context of several particle pair production hypotheses.

2   The ALEPH detector

A detailed description of the ALEPH detector can be found in Ref. [1] and of its performance in Ref. [2]. Charged particles are detected in the central part of the detector consisting of a vertex detector, a cylindrical drift chamber and a large time projection chamber, which together measure up to 31 coordinates along the charged particle trajectories. A 1.5 T axial magnetic field is provided by a superconducting solenoidal coil. A $1/p_T$ resolution of 6×10^{-4} $(GeV/c)^{-1}$ is achieved.

Electrons and photons are identified in the electromagnetic calorimeter by their characteristic longitudinal and transverse shower developments. The calorimeter, a lead/wire-plane sampling device with fine read-out segmentation and total thickness of 22 radiation lengths at normal incidence, provides a relative energy resolution of $0.18/\sqrt{E}$ (E in GeV).

Muons are identified by their characteristic penetration pattern in the hadron calorimeter, a 1.2 m thick yoke instrumented with 23 layers of streamer tubes, together with two surrounding layers of muon chambers. In association with the electromagnetic calorimeter, the hadron calorimeter also provides a measurement of the energy of charged and neutral hadrons with a relative resolution of $0.80/\sqrt{E}$ (E in GeV).

The total visible energy, and therefore also the missing energy, is measured with an energy-flow reconstruction algorithm [2] which combines all of the above measurements, supplemented by the energy detected at low polar angle (down to 24 mrad from the beam axis) by two additional electromagnetic calorimeters which are used principally for the luminosity determination. In addition to the total energy measurement, the energy-flow reconstruction algorithm also provides a list of charged and neutral reconstructed objects, called *energy-flow particles*, allowing jets to be reconstructed with an angular resolution of 20 mrad both for the

polar and azimuthal angles, and a relatively uniform energy resolution over the whole detector acceptance. The latter can be parameterized as $\sigma_E = (0.60\sqrt{E} + 0.6)$ GeV $\times (1 + \cos^2\theta)$ where E (in GeV) and θ are the jet energy and polar angle, respectively.

Finally, jets originating from b quarks are identified from lifetime b-tagging algorithms [3]. These algorithms make use of a new vertex detector installed in October 1995, twice as long as the former one thus extending the acceptance to lower polar angles, and with similar performance [2].

3 Four-jet events

3.1 The four-jet topology selection

The selection criteria were tailored to minimize the expected standard model backgrounds while preserving a high efficiency for an $e^+e^- \rightarrow hA$ signal, simulated with the HZHA event generator [4]. The standard processes expected to contribute to the four-jet topology were simulated with PYTHIA 5.7 [5], thus neglecting the small interference terms in the four-fermion final state:

(i) 140,000 $e^+e^- \rightarrow q\bar{q}$ events, generated according to the parton shower evolution option of JETSET 7.4 [5], corresponding to approximately 80 times the recorded luminosity;

(ii) 1800 events from $e^+e^- \rightarrow ZZ$, $Z\gamma^*$, $\gamma^*\gamma^* \rightarrow$ four-fermion final states, representing almost 60 times the data sample;

(iii) 100 events from $e^+e^- \rightarrow WW \rightarrow$ four-fermion final states, corresponding to over 125 times the recorded luminosity.

As a preselection, only events compatible with a hadronic final state are kept. It is required that at least eight charged particle tracks be reconstructed with at least four hits in the time projection chamber, with a polar angle with respect to the beam such that $|\cos\theta| < 0.95$, and originating from within a cylinder of length 20 cm and radius 2 cm coaxial with the beam and centred at the nominal collision point. In addition, the scalar sum of the charged particle momenta must exceed 10% of the centre-of-mass energy.

To reject events with a real Z and large initial state radiation, hereafter called radiative returns to the Z, in which the photon escapes undetected along the beam, the missing momentum measured along that direction is required to be smaller than $0.75 \times (m_{\mathrm{vis}} - 90)$, where m_{vis} is the invariant mass (in GeV/c^2) of the system formed by all energy-flow particles. This criterion also rejects the remaining events from $\gamma\gamma$ collisions.

Events are then clustered into jets of particles with the Durham algorithm [6], operated with a y_{cut} value of 0.008, chosen to maximize the signal-to-noise ratio in the four-jet topology: the $e^+e^- \rightarrow q\bar{q}$ contribution rapidly increases for smaller y_{cut} values due to many three-parton events actually clustered into four jets, and the $e^+e^- \rightarrow hA$ efficiency decreases for larger y_{cut} values leading to a larger fraction of events reconstructed with only three jets. Events which the Durham algorithm reconstructs with fewer than four jets are reclustered with the

JADE algorithm [7] with a y_{cut} value of 0.022, leading to a 10% increase in efficiency without decreasing the signal-to-noise ratio. Events still reconstructed with fewer than four jets are rejected. Events with five jets (7.5% of the simulated $q\bar{q}$ events) are clustered down to four jets by merging the two jets with the smallest invariant mass. With such high y_{cut} values, no events are expected to be reconstructed with six or more jets, and none are found.

Radiative returns to the Z with an initial state radiation photon emitted within the detector acceptance are reduced by requiring that none of the four jets contains more than 80% electromagnetic energy. Here, the electromagnetic energy is defined as the energy measured in one of the luminosity calorimeters, the energy of the identified photons, electrons and positrons, and the energy measured in the hadron calorimeter behind the cracks of the electromagnetic calorimeter. Furthermore, all four jet masses, computed assuming charged particles to be pions and neutral particles to be massless, must exceed 1 GeV/c^2.

The energies of the four jets are subsequently rescaled by imposing total energy-momentum conservation with the assumption that the four jet velocities $\vec{\beta_i} = \vec{p_i}/E_i$ are perfectly measured. To ensure the compatibility of the events with the four-body hypothesis, the recomputed energies are required to be positive.

Events from $e^+e^- \rightarrow q\bar{q}gg$ and $e^+e^- \rightarrow (Z \rightarrow q\bar{q}g)(\gamma^* \rightarrow q\bar{q})$ processes usually have two clearly leading jets and two less energetic (from radiated gluons) and/or less massive (from virtual photon) jets. To reduce this contribution, it is required that all di-jet masses (as computed from the rescaled energies) exceed 25 GeV/c^2, the sum of the masses of the two lightest jets be larger than 10 GeV/c^2, and the sum of their charged particle multiplicity be at least ten.

Table 1: Numbers of events observed in the data and expected from the different standard processes at the various stages of the selection. Here ZZ includes the $e^+e^- \rightarrow$ ZZ, γ^*Z and $\gamma^*\gamma^*$ processes. Also shown is the evolution of the selection efficiency for $e^+e^- \rightarrow$ hA $\rightarrow b\bar{b}b\bar{b}$.

Criterion	Data	$q\bar{q}$	ZZ	WW	Total	hA
Hadronic final state	1839	1627	17	0.7	1830*	99.8%
No radiative return	769	780	12	0.5	793	92.4%
At least four jets	153	137	3.3	0.3	141	69.8%
No γ-like jets	37	30.4	1.8	0.25	32.4	67.8%
Four-body compatibility	35	28.2	1.7	0.25	30.1	65.6%
Large di-jet masses	22	14.9	1.2	0.19	16.3	55.0%
Large jet masses	19	11.1	0.50	0.14	11.7	48.6%
Large multiplicities	16	8.3	0.21	0.08	8.6	42.0%

The contribution of the $\gamma\gamma$ processes is estimated from the data to be ~ 185 events at the level of the first cut. It becomes negligible after the anti-radiative return criterion.

The numbers of events observed in the data and expected from standard processes are shown in Table 1 together with the efficiency estimated from a Monte Carlo sample of 500 hA $\rightarrow b\bar{b}b\bar{b}$ events ($m_h \simeq m_A = 55$ GeV/c^2) at the various stages of the selection. In this table, the numbers of $q\bar{q}$, ZZ and WW events refer to the simulation made using PYTHIA followed

by parton shower evolution. At the end of the selection procedure, 16 events are selected in the data while 8.6 ± 0.3 (stat.) are expected from the standard processes, corresponding to a Poisson probability of 1.5%. In this sample, three events are originally reconstructed with five jets (1.7 five-jet events out of 16 are expected from standard processes) and only one event is reconstructed with the JADE jet clustering (1.9 events expected).

3.2   The invariant mass distribution

In addition to an overall excess of events, the production of two equal (or slightly different) mass objects is also expected to be clearly seen in the distribution of the sum ΣM of the two di-jet masses for the jet pair combination (out of three) with the smallest di-jet mass difference ΔM. As an illustration, the distribution of ΣM is shown in Fig. 1a for hA simulated events with $m_h = m_A = 55$ GeV/c^2 and with negligible intrinsic widths, after the energy rescaling is applied.
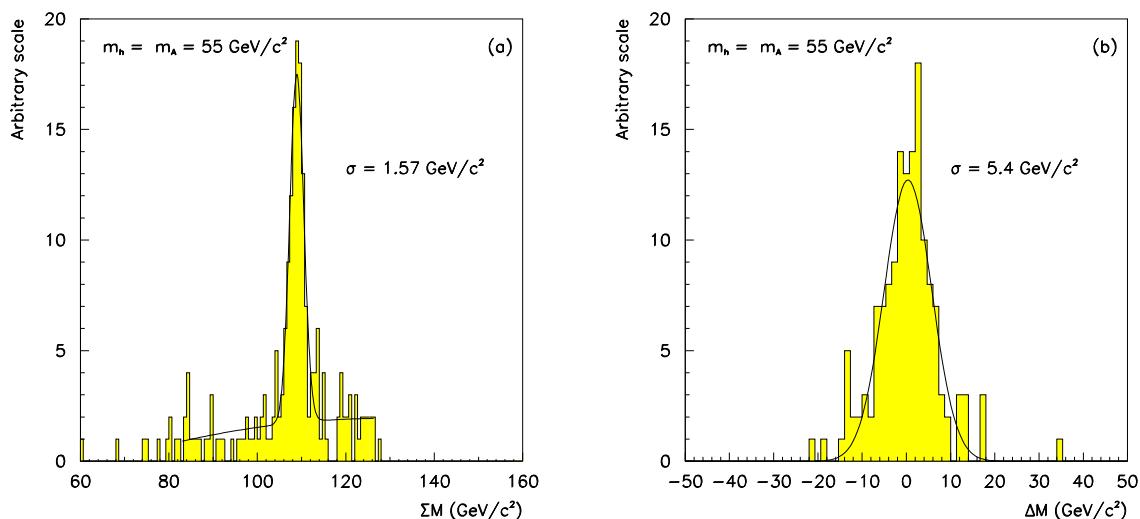

Figure 1: Distributions of the di-jet mass sum (a) and difference (b) of the jet pair combination with the smallest mass difference for hA simulated events with $m_h = m_A = 55$ GeV/c^2 and with negligible intrinsic widths. Also shown (curve) is a fit of a Gaussian to these distributions and the resulting resolution. The non-Gaussian tails of the mass sum distribution are fitted to a second order polynomial.

This distribution shows a peak and non-Gaussian tails due to events in which the jet pairing with the smallest di-jet mass difference is not the right combination (see Section 3.4). The peak is fitted with a Gaussian of mean value 109 GeV/c^2 and a σ of approximately 1.6 GeV/c^2. About 60% of the events coming from $e^+e^- \rightarrow$ hA are expected to be found within $\pm 2\sigma$ around this mean value. The resolution on the di-jet mass difference of the events contained in the peak is 5.4 GeV/c^2 (Fig. 1b). The difference between the two resolutions is a purely kinematical effect induced by the rescaling, and would be maximal at the production threshold (infinitely good mass sum resolution, no mass difference resolution). When the rescaling procedure is not applied, the di-jet mass sum distribution is centred around 103 GeV/c^2, with a resolution of 9 GeV/c^2. The same resolution is obtained for the di-jet mass difference.

4
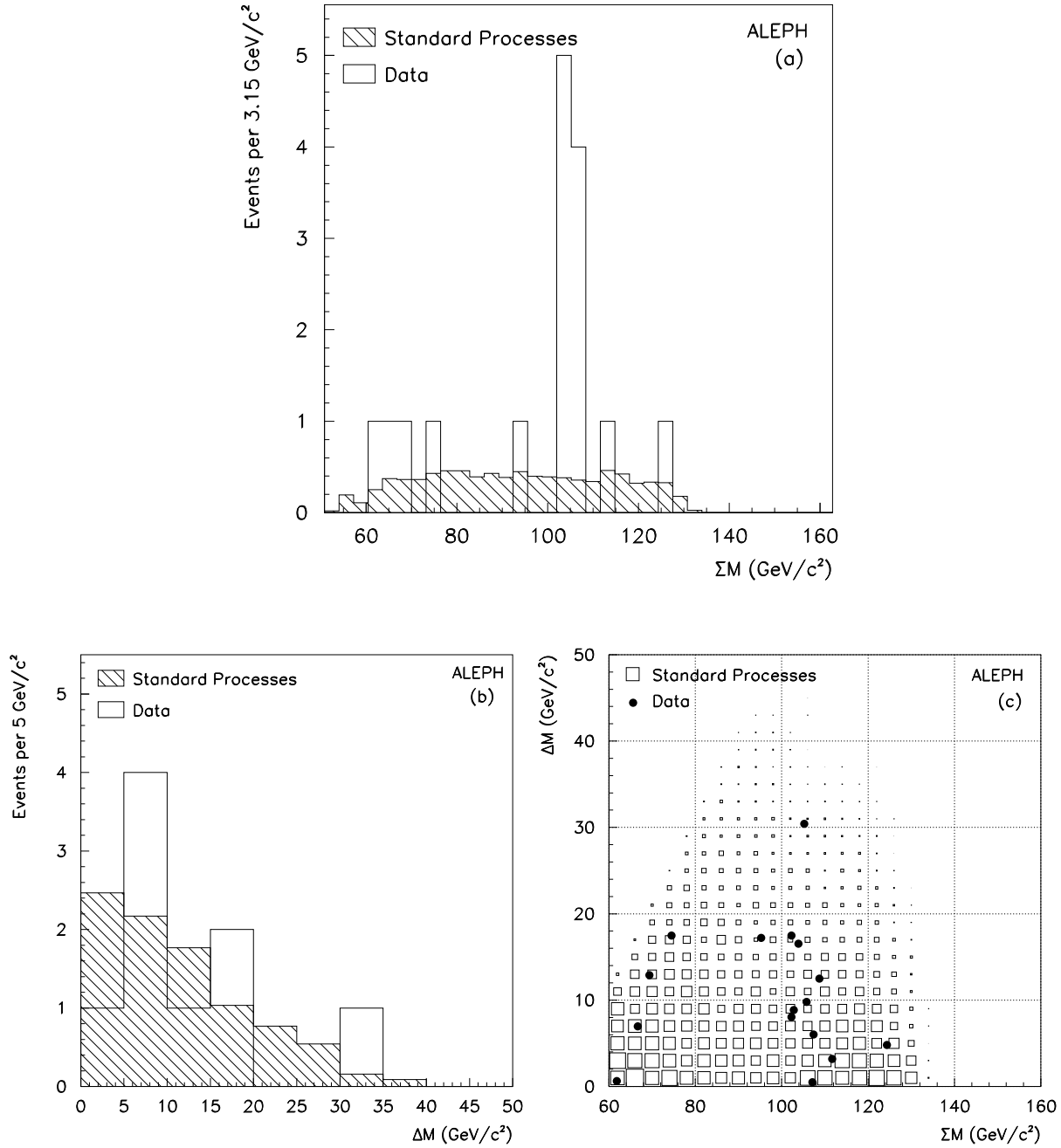
Figure 2: (a) Distribution of the sum of the di-jet masses for the combination with the smallest mass difference for the data (histogram). The hatched histogram is the distribution expected from a simulation of the standard processes. The width and the origin of the bins are chosen as explained in the text. (b) Distribution of the absolute value of the di-jet mass difference for the nine events clustering around 105 GeV/c^2 for the data (histogram) and the simulation of standard processes normalized to nine events (hatched histogram). (c) Distribution of the difference vs the sum of the two di-jet masses for the data (points) and as expected from standard processes (boxes).

5

The distribution of the mass sum obtained in the data is shown in Fig. 2a, together with the standard model expectation. The width of the bins is defined to correspond to twice the expected resolution on ΣM (*i.e.* 3.15 GeV/c^2), and their origin is deliberately chosen to maximize the number of events found in any two consecutive bins. (The probability presented below is consistently computed by following the same prescriptions on toy Monte Carlo experiments.) While the mass distribution from the standard processes is expected to be quite flat over the whole mass interval, the data show an accumulation of nine events in two bins around 105 GeV/c^2. The presence of this accumulation is robust against changes of jet algorithm (JADE *vs* Durham), of y_{cut} value, and of specific cuts aimed at reducing the contributions of the QCD and four-fermion processes. Independently of the overall excess of events in the data (16 events observed with 8.6 expected), the probability that 16 events produce such an accumulation or larger in any 6.30 GeV/c^2-wide interval is 0.01%.

The distribution of the di-jet mass difference is displayed for the nine events in Fig. 2b, together with the standard model expectation (normalized to nine events). The compatibility of this distribution with standard processes and various pair production hypotheses is discussed in Section 5.4. Finally, the correlation between the di-jet mass difference and the di-jet mass sum is shown in Fig. 2c.

3.3   Systematic checks

In order to check that the apparent excess is not due to an underestimation of the cross-section for any of the standard processes, and that the accumulation in the di-jet mass sum distribution is not an artifact of the selection or the rescaling procedure, of detector geometry or of unexpected detector effect, a number of systematic studies have been performed.

In Section 3.3.1, the jet angular distribution is examined and the rescaled jet energies are compared to the measured ones. These basic checks address the question of detector effects, possibly further enhanced by the rescaling procedure. The expectation from the $e^+e^- \to q\bar{q}$ process, for both the total cross section and the shape of the di-jet mass sum distribution, is studied in Section 3.3.2. The reliability of the simulation from PYTHIA followed by a parton shower evolution is tested for all the quantities used in the selection procedure. Similarly, the simulation of the four-fermion final state by PYTHIA is studied in Section 3.3.3. Given its very small cross section, the $e^+e^- \to WW$ background cannot be expected to produce any substantial effect and is not considered in these systematic checks.

3.3.1   Jet energy and angular distributions

The di-jet invariant mass determination depends on the rescaling procedure (see Section 3.1) which uses the jet directions but not directly the measured jet energies. As a check, the distribution of the azimuthal angle φ *vs* the cosine of the polar angle θ for the jets of the 16 events is displayed in Fig. 3a. No particular enhancement is visible in this distribution.

The reliability of the rescaling procedure can be further tested by comparing the measured jet energies E_{meas} to the rescaled energies E_{resc}. Any significant missing or additional energy caused for example by detector problems or initial state radiation would be seen as large
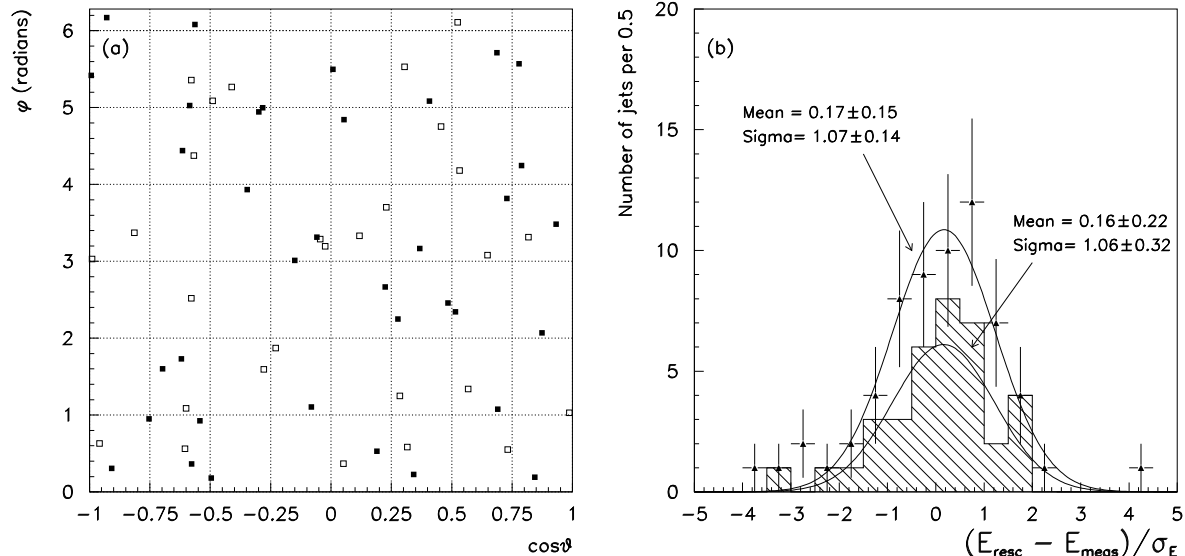
Figure 3: (a) φ vs $\cos\theta$ distribution for the jets of the 16 events (four entries per event). The black squares represent the jets from the nine events around 105 GeV/c^2, and the empty squares those of the seven other events. (b) Distribution of $(E_{\rm resc} - E_{\rm meas})/\sigma_E$ for the jets of the 16 events (four entries per event). The hatched histogram refers to the nine events around 105 GeV/c^2, and the curves indicate the result of Gaussian fits.

positive or negative tails in the distribution of $(E_{\rm resc} - E_{\rm meas})/\sigma_E$, where σ_E is the jet energy resolution. The distributions are shown in Fig. 3b for all selected events and for the nine events around 105 GeV/c^2. They are in agreement with each other, and in reasonable agreement with a Gaussian. In addition, the mean value of the total missing energy is measured to be 4.0 ± 1.3 GeV/c^2 in the data, in agreement with the expectation of 4.0 ± 0.4 GeV/c^2 for standard four-jet events.

3.3.2 Expectations from $e^+e^- \rightarrow q\bar{q}$

In Section 3.1, the number of events expected from $e^+e^- \rightarrow q\bar{q}$ is determined by applying the selection procedure to the sample generated by PYTHIA with the parton shower option of JETSET (hereafter simply called JETSET). Although it is known to predict the charged particle multiplicity and the three-, four- and five-jet rates over a very large Q^2 range, the parton shower evolution might well be inaccurate in this particular phase space region (four well defined jets), both for the normalization and for the invariant mass distribution.

Therefore, a sample of 9,600 $q\bar{q}$ events simulated with the exact O(α_s^2) QCD matrix element, expected to produce the correct rate and kinematics for the four-parton final state (but not for five or more partons), was processed through the same selection chain. These events were generated after tuning the two parameters a and b of the Lund symmetric fragmentation function [5] from 1.0 and 0.496 (their values at $\sqrt{s} = 91.2$ GeV) to 1.1 and 0.4 respectively, so as to reproduce the mean charged multiplicity observed for $q\bar{q}$ events at $\sqrt{s} = 133$ GeV [8]. A total of 9.0 ± 0.9 events is predicted, in agreement with the JETSET prediction of 8.6 ± 0.3 events.

7

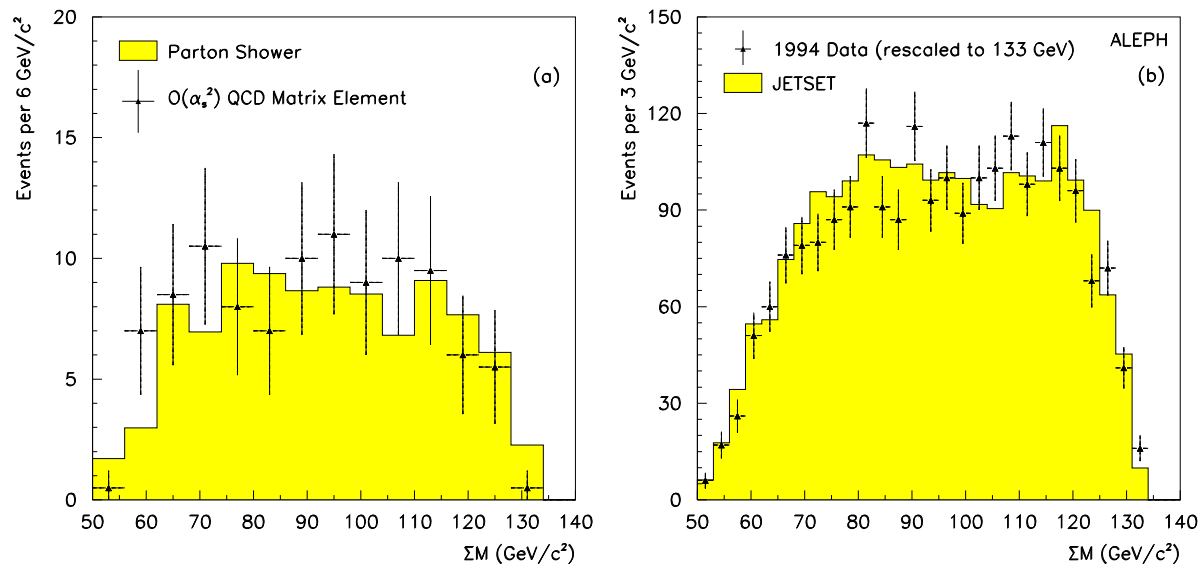The two di-jet mass sum distributions are also compatible within the statistical uncertainties, as shown in Fig. 4a.

Figure 4: Di-jet mass sum distributions: Comparison of the JETSET parton shower evolution predictions to (a) the α_s^2 QCD matrix element prediction at a centre-of-mass energy of 133 GeV; and (b) 100,000 hadronic events collected at the Z peak in 1994 with energies rescaled to 133 GeV.

To further check that JETSET adequately simulates the four-jet topology, the same analysis has been applied to simulated and real data at $\sqrt{s} \sim m_Z$. To make the comparison easier, the total energy is still constrained to 133 GeV in the jet energy rescaling procedure. (This is equivalent to rescaling the various energy-dependent cuts to the centre-of-mass energy.) As a consequence, any geometrical effect would appear at the same place in the di-jet mass sum distribution independently of $\sqrt{s}$. The anti-radiative return criterion, no longer justified, is removed and the last requirement on the jet charged multiplicity is relaxed by one unit, according to the evolution of this quantity between 133 and 91 GeV. Three event samples are studied:

(i) a Monte Carlo sample of 422,000 hadronic Z decays, simulated with JETSET;

(ii) a first data sample equivalent to approximately 110,000 hadronic Z decays collected at the end of 1994, to check the reliability of the JETSET simulation;

(iii) a second data sample of 1362 Z → q$\bar{\text{q}}$ events, collected in October 1995 just prior to the LEP energy increase to 130 GeV, aimed at checking the absence of detector effects related to the new configuration, used at high energy.

The numbers of events expected and observed in the two samples are displayed in Table 2, after each step of the selection. No significant excess is observed with respect to the standard expectation, either in 1994 or in 1995. In particular, the rejection power of the two last cuts,

8

closely related to the jet structure and therefore particularly dependent on the reliability of the hadronization step of the simulation, seem to be reasonably reproduced by the Monte Carlo. Although slightly lower in the data, the overall selection efficiency is in agreement with the simulation within one standard deviation. This possible systematic effect is conservatively ignored.

Table 2: Numbers of events expected and observed in the data collected at the Z peak, in 1994 and in 1995 (see text).

	1994 sample		1995 sample	
Criterion	Expected	Observed	Expected	Observed
Hadronic final state	105503	104677	1316	1308
At least four jets	7311	7362	91	98
No γ-like jets	6620	6594	83	91
Four-body compatibility	6256	6202	78	86
Large di-jet masses	3292	3339	41	52
Large jet masses	2802	2808	35	46
Large multiplicities	1861	1803	24	27

The di-jet mass sum distribution of the 1994 sample is shown in Fig. 4b, together with the expected distribution. The data agree with the Monte Carlo expectation, thus validating the simulation of the four-jet topology. The distributions predicted at 133 GeV (Fig. 4a) and at 91 GeV (Fig. 4b) are also very similar. The di-jet mass sum distribution of the October 1995 sample is shown in Fig. 5a with the same binning as in Fig. 2 to permit direct comparison. No structure is visible around 105 GeV/c^2 (one event observed with approximately two expected).

To conclude, the accumulation observed at high energy cannot be explained either by a detector imperfection, by a geometrical effect, or an inadequacy of the simulation of the $e^+e^- \rightarrow q\bar{q}$ process.

3.3.3 The $e^+e^- \rightarrow$ four-fermion final state

The four-fermion final state is produced in PYTHIA *via* the so-called double conversion processes $e^+e^- \rightarrow ZZ$ (where Z is a generic notation for a Z boson or a virtual photon) and $e^+e^- \rightarrow WW$. The numbers of events expected from these two processes are respectively 0.21 ± 0.04 and 0.08 ± 0.02 when all cuts are applied (see Table 1). However, the four-fermion final state may arise from a variety of non-resonant diagrams involving photon, Z and W exchange. Although the cross section is expected to be dominated by the double conversions, the additional diagrams may have a non-negligible contribution. The FERMISV generator [9] is well suited to evaluate the effects of the diagrams involving only photon and Z exchange, together with those of the QCD corrections, which are important when a virtual photon turns into a q$\bar{q}$ pair [10]. One thousand $e^+e^- \rightarrow u\bar{u}d\bar{d}$ events were generated with FERMISV. After the analysis is applied, 0.18 four-fermion events are predicted from FERMISV, compatible with the 0.21 events expected from the $e^+e^- \rightarrow ZZ$ simulation in PYTHIA.
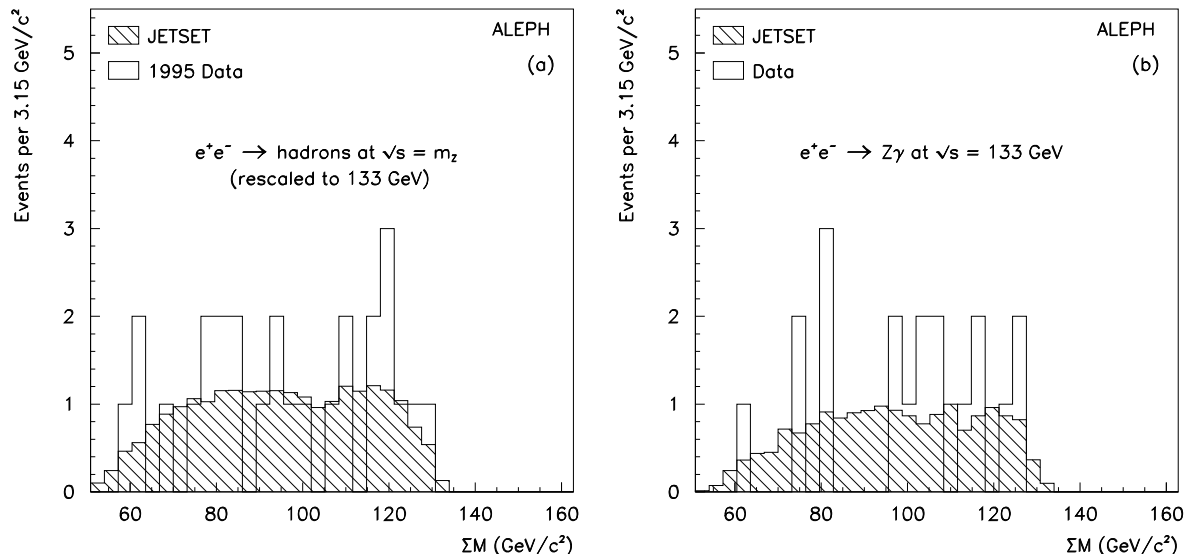
9

Figure 5: Distribution of the sum of the di-jet masses for the combination with the smallest mass difference (a) for the 1995 data collected at the Z peak just prior to the high energy run (the total energy is rescaled to 133 GeV); and (b) for the $e^+e^- \to Z\gamma$ events collected during the high energy run. The hatched histograms are the distributions expected from JETSET.

The simulation can also be tested directly with the high energy data in the following way. After all cuts, the dominant diagram from four-fermion processes is $e^+e^- \to Z\gamma^*$, with the Z decaying into $q\bar{q}g$ and the virtual photon producing a low mass $q\bar{q}$ system which is subsequently reconstructed as a single jet. Therefore, systematic uncertainties on the cross section and on the di-jet mass sum distribution can be evaluated with the $e^+e^- \to Z\gamma$ process, the real photon playing the rôle of one of the four jets. A selection procedure similar to that described in Section 3.1 is applied to the data and the 140,000 $q\bar{q}$ events simulated at high energy. At least one γ-like jet (instead of none) with mass smaller than 200 MeV/c^2 is required, and this jet is ignored in the last two requirements related to the jet masses and multiplicities. A total of 19 such events are found in the data, to be compared to the expectation of 17.4 ± 0.5 events. The mass sum distribution of these 19 events does not exhibit any significant structure around 105 GeV/c^2 (four events observed with approximately two expected), as can be seen in Fig. 5b. Therefore, the four-fermion final state cannot be responsible for the excess and the accumulation observed in the four-jet topology.

3.4 Off-peak events

Since no systematic bias has been found to explain the event accumulation around 105 GeV/c^2, the pair production hypothesis can be reconsidered. As shown in Section 3.2, only part of the events originating from particle pair production are expected to be found in a 6.30 GeV/c^2-wide interval of the di-jet mass sum distribution. Consequently, a fraction of the seven data events observed outside the di-jet mass sum peak of Figure 2 are expected to come from the same source as the events around 105 GeV/c^2.

10

As already mentioned, the non-Gaussian tails of the di-jet mass sum distribution of Fig. 1a, containing 40% of the selected $e^+e^- \rightarrow hA$ sample, are mainly due to events in which the jet pairing with the smallest di-jet mass difference is not the right combination. For these hA events, the expected distribution of the di-jet mass sum for the jet pairing with the second-smallest di-jet mass difference is actually very similar to the distribution of Fig. 1a, with about 60% of the events within ± 3.15 GeV/c^2 of 109 GeV/c^2.

The same procedure can be applied to the data and to the standard process simulated events: the events populating the two bins of the peak of Figure 2 are removed from the data and the Monte Carlo samples and the distribution of the di-jet mass sum of the jet pairing with the second-smallest di-jet mass difference is built for the remaining events. This distribution is shown in Fig. 6 with the same binning definition as in Fig. 2. The simulated sample is normalized to seven events.
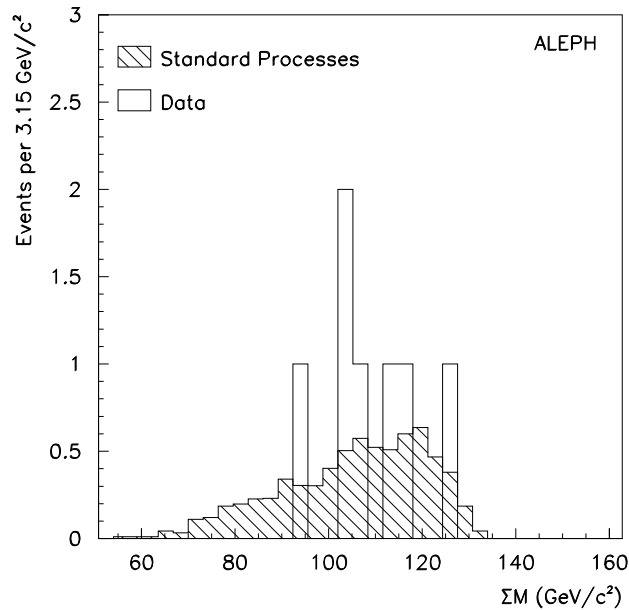

Figure 6: Distribution of the di-jet mass sum for the combination with the second-smallest mass difference in the data, once the nine events around 105 GeV/c^2 are removed. The hatched histogram is the distribution expected from the simulation of the standard processes, obtained with the same procedure and normalized to seven events.

Three events are found in the same two bins as before, with di-jet mass sums 104.7, 105.2 and 106.0 GeV/c^2, while 1.02 ± 0.04 (out of seven) are expected from standard processes.

The question of the overall compatibility of Fig. 2 and Fig. 6 with the simultaneous production of standard four-jet events and of a pair of heavy particles can be addressed in the following way (see also Table 3). The total number of selected events that can be attributed to the possible signal is unknown. The best estimate of this number is given by the overall excess of events with respect to the standard model expectation, *i.e.* $16 - 8.6 = 7.4$ events. In the hypothesis of equal masses, a total of 5.2 events (60% of the signal and 0.8 events from standard processes) is therefore expected in two consecutive bins of the di-jet mass sum distribution for the jet pairing with the smallest mass difference. Similarly, 3.0 events are expected in the

11

same bins of the di-jet mass sum distribution for the jet pairing with the second-smallest mass difference (of which 1.2 come from standard processes), and 7.8 events are expected outside these two bins in both distributions (of which 6.6 come from standard processes). The probability to observe an equally or more unlikely distribution of the numbers of events in the three samples (9, 3 and 4 events are observed while 5.2, 3.0 and 7.8 are expected) is 10%.

Table 3: Numbers of events expected from standard processes and from a possible equal-mass pair-produced particle signal; and numbers of events observed in the data: in the peak from the smallest di-jet mass difference, in the peak from the second smallest di-jet mass difference, and off-peak.

	Standard processes	"Signal"	Total expected	Total observed
Smallest ΔM peak	0.8	4.4	5.2	9
Second smallest ΔM peak	1.2	1.8	3.0	3
Off-peak	6.6	1.2	7.8	4

In the rest of the paper, the 12 (= 9 + 3) events clustering in di-jet mass sum around 105 GeV/c^2 are further studied and are called "peak events" for convenience. Among these peak events, 2.0 are expected to arise from standard processes. The relevant properties of these 12 events are given in Section 5.

4 A comparison with QCD

The next step of investigation involves a systematic comparison of the four-jet sample with the standard process (mainly QCD) predictions, ignoring the overall excess of events observed after a specific selection, and that 12 of the selected events are clustered in mass within the detector resolution. If these 12 peak events are due to a statistical fluctuation, their properties should not differ from those of standard four-jet events.

In the following two sections, the last three cuts, specifically aimed at enriching the four-jet sample in $e^+e^- \rightarrow hA$ signal and therefore questionable in an unbiased comparison with standard processes, are removed. The resulting sample of 35 four-jet events (see Table 1) is compared with the predictions of the standard model in two respects: *(i)* the event dynamics at the parton level; and *(ii)* the jet structure itself. The overall compatibility with the standard processes of these 35 events is addressed in Section 4.3.

In addition, the properties of the 12 peak events and of the other 23 events, hereafter called side-band events, are also compared in Section 4.3. With the same hypothesis as in Section 3.4, 5.3 of these side-band events are in fact expected to come from the same source as the peak events. Of those 5.3 events, 1.2 belong to the final selection (see Table 3) while 4.1 are due to the efficiency increase brought by the removal of the three last cuts. Of those 4.1 events, only 2.2 are expected to fall in the same di-jet mass sum region as the peak events.

4.1 The parton dynamics

A simple way to combine all the information concerning the dynamics of an event is to determine its matrix element squared for the process considered [11]. Here, what matters is the four-parton QCD matrix element computed at order α_s^2. Calculations of this matrix element squared exist [12] which are already integrated over the event direction, *i.e.* over variables not related to QCD but to the electroweak production process $e^+e^- \rightarrow q\bar{q}$. After this integration the matrix element squared is, up to multiplicative factors, independent of the centre-of-mass energy when computed at the Born level.

For a given event, the parton type (quark or gluon) and parton four-momenta, which can be approximated by the jet energies and directions, are needed to compute the matrix element. Since $q\bar{q}q\bar{q}$ and $q\bar{q}gg$ final states cannot easily be disentangled experimentally, the matrix element squared is summed over all the possible parton types. Still, some ambiguities remain as long as the parton ordering (depending on the quark/antiquark/gluon identification too) is unknown. A possible solution to this problem would be to average the matrix element squared over the 24 possible parton orderings, but this would unavoidably lead to a dilution of the information. It is therefore preferable to choose the "most QCD-like" combination, i.e. the parton ordering giving the highest matrix element squared.

Four-jet events arising from QCD tend to be produced where the QCD cross section, or the QCD matrix element, is largest, namely close to the poles of QCD. Since these poles are not likely to be present in any exotic processes, events produced by such a process would rather populate the low values of the QCD matrix element squared distribution. The distribution of the logarithm of this matrix element squared is shown for the data in Fig. 7, together with the standard prediction. An idea of its discriminating power is given in Table 4 where the mean values and the RMS of the corresponding distributions for various processes are shown.

Table 4: Mean, RMS and most likely (MLV) values of the distribution of the logarithm of the QCD matrix element squared for $e^+e^- \rightarrow q\bar{q}$, ZZ, WW and hA.

Process	Mean	RMS	MLV
$e^+e^- \rightarrow q\bar{q}$	2.80	0.46	2.72
$e^+e^- \rightarrow ZZ$	2.57	0.34	2.48
$e^+e^- \rightarrow WW$	2.51	0.30	2.40
$e^+e^- \rightarrow hA$	2.36	0.37	2.17

A possible excess of events appears where exotic events are expected to show up: eleven events are observed below 2.36 (this is the mean value expected for $e^+e^- \rightarrow hA$) to be compared to the standard prediction of 5.2 events. To check the reliability of the standard process simulation in this region on the one hand, and the absence of additional detector effects in the high energy run on the other, the distributions of the QCD matrix element squared for data samples *(ii)* and *(iii)* of Section 3.3.2 are compared to the QCD prediction from JETSET in Fig. 8a and 8b. The two data samples agree with each other and with the simulation: no particular excess can be noticed at low matrix element squared values.
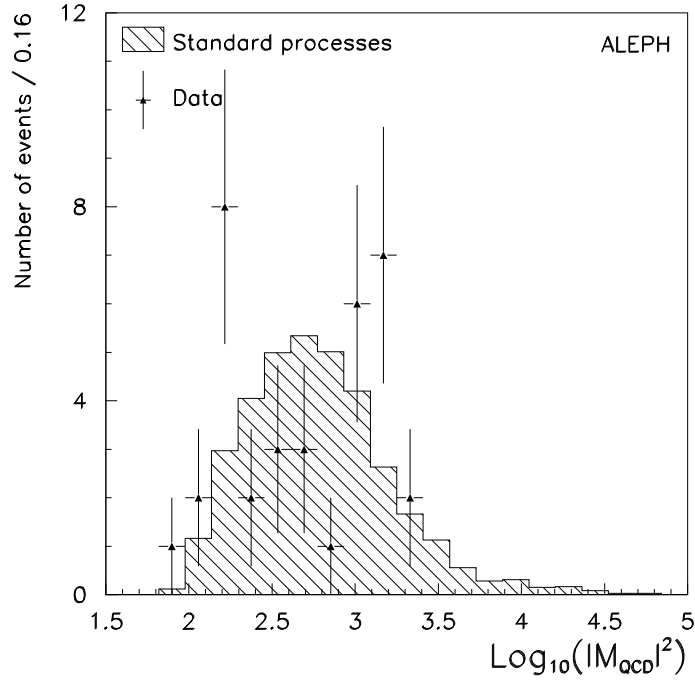
Figure 7: Distribution of the logarithm of the QCD matrix element squared for the data (triangles with error bars), and the standard process prediction normalized to 35 events.
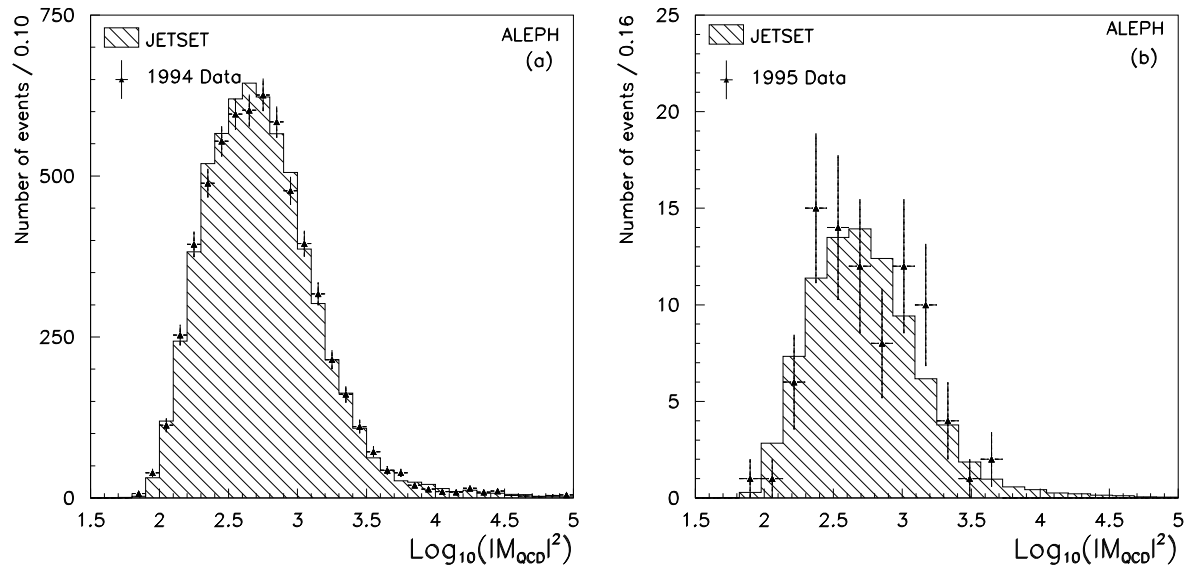

Figure 8: Distribution of the QCD matrix element squared for four-jet events (a) in 1994 and (b) in 1995 prior to the high energy run. The hatched histogram is the prediction from JETSET.

4.2 The jet charge

In ALEPH, jet charge has been used to statistically measure the charge content of the primary partons [13]. Here, it is used to distinguish between q̄qgg final states, known to occur in more than 90% of the QCD-produced four-jet events [14], and four-quark final states often expected in the hadronic decays of pair-produced particles. Other quantities were tried such as jet multiplicities, jet masses, and rapidity distributions [15], but they were found not to be effective in discriminating between quark and gluon jets for such a wide jet energy spectrum. A rapidity-weighted jet charge is used, defined for each jet as [16]

$$Q_{\mathrm{jet}} = \sum_{i=1}^{N} y_i Q_i / \sum_{i=1}^{N} y_i,$$

where the sums extend over the N charged particles of the jet, Q_i being the electric charge and y_i the rapidity with respect to the jet direction, of the charged particle i. Table 5 shows the mean value and the RMS of the jet charge distributions determined for each parton flavour in simulated four-jet events.

Table 5: Mean and RMS values of the jet charge distribution for each parton flavour in simulated four-jet events.

Flavour	Mean	RMS
u quarks	+0.14	0.22
d quarks	−0.09	0.22
s quarks	−0.09	0.22
c quarks	+0.10	0.20
b quarks	−0.06	0.19
gluons	+0.01	0.23

Since final states produced by QCD contain two gluon jets most of the time, the smallest of the four jet charges in absolute value, denoted $|Q|_{\mathrm{min}}$, is expected to be smaller than that obtained in four-quark final states. The distribution of the smallest jet-charge, in absolute value, is shown in Fig. 9 both for the data and the standard model prediction. Here again, an excess of events with respect to the expectation can be noticed for $|Q|_{\mathrm{min}}$ values above ~ 0.10 (16 events observed for 6.0 expected).

To check the reliability of the detector simulation in this respect, it is compared to to the 1994 and 1995 data samples of Section 3.3.2, as presented in Fig. 10a and 10b. Again, the two data samples agree with each other and with the simulation: no particular excess can be noticed at high $|Q|_{\mathrm{min}}$ values.

4.3 Compatibility with the standard predictions

The two excesses observed at low matrix element squared and high jet charge values might well be *(i)* two uncorrelated statistical fluctuations (*i.e.* not affecting the same events); and
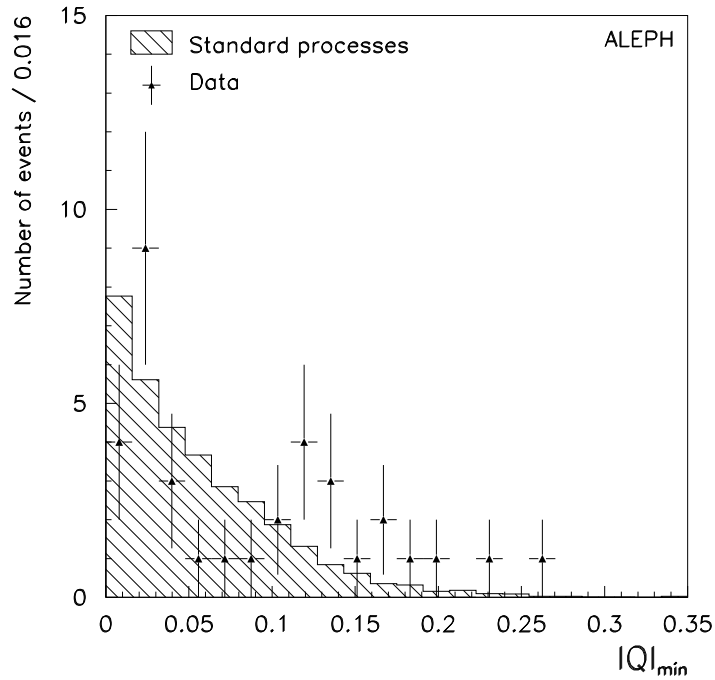
Figure 9: Distribution of the smallest of the four jet charges, in absolute value, for the data (triangles with error bars) and the standard model prediction (hatched histogram), normalized to 35 events.
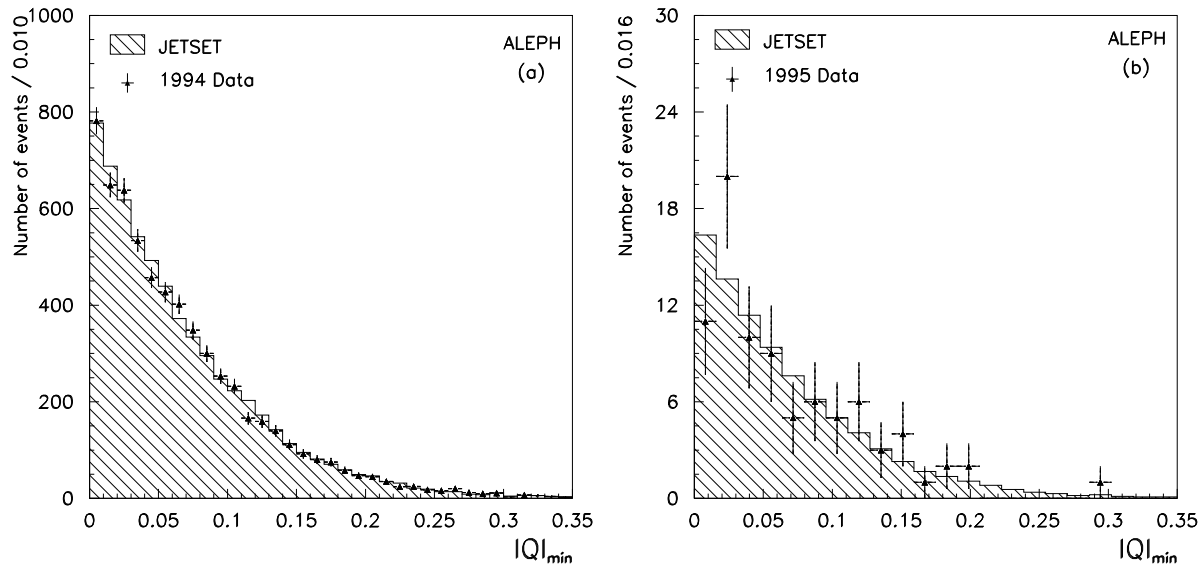

Figure 10: Distribution of the smallest of the four jet charges for four-jet events (a) in 1994 and (b) in 1995 prior to the high energy run. The hatched histogram is the QCD prediction from JETSET.

16

(ii) not related to the 12 peak events. In addition, since the QCD matrix element squared is not identical for $q\bar{q}q\bar{q}$ and $q\bar{q}gg$ final states, the expected parton dynamics and parton flavours might not be completely uncorrelated. (It has actually been checked that the matrix element squared, when summed over all parton types as explained in Section 4.1, is on average slightly larger for $u\bar{u}u\bar{u}$ events than for a normal flavour mixture of four-jet events.)

To check and quantify the first point, it is interesting to combine these two quantities into a single variable since two uncorrelated fluctuations would tend to compensate each other when combined, while the effect would be enhanced if they involve the same events. The method used for the combination and for the determination of the related probabilities is described in Section 4.3.1. The result of this combination is shown in Section 4.3.2 for the 35 events on the one hand, and for the peak and side-band events separately on the other. Finally, systematic uncertainties related to the simulation and to the method are studied in Section 4.3.3.

4.3.1   Combination and probabilities

The combination of the parton dynamics and the parton flavour information is performed in the following way [17]. Exotic four-quark events are expected to be found at small $|M_{\text{QCD}}|^2$ and/or large $|Q|_{\min}$ values. Therefore, for each event (data or Monte Carlo), the fraction f of $e^+e^- \rightarrow q\bar{q}$ simulated events with a lower matrix element squared value and a larger $|Q|_{\min}$ value than its own is determined. The probability of this event, hereafter called rarity, is defined as the fraction r of $e^+e^- \rightarrow q\bar{q}$ simulated events with a value of f smaller than its own.

By construction, the distribution of r is uniformly distributed between 0 and 1 for $e^+e^- \rightarrow q\bar{q}$ simulated events, while it is expected to be peaked at 0 for more exotic four-jet final states. For example, the rarity distribution obtained for the standard four-fermion final state is slightly biased towards small values. This direct event counting method takes into account all expected correlations between the two variables.

An accumulation observed in the data at small rarity values has always a non-zero probability of being due to a statistical fluctuation. The corresponding probability can be evaluated from the data with the mean value E (hereafter called exoticness) of the quantity $\sqrt{N_{\text{obs}}} \times (1 + \log r)$, where N_{obs} is the number of events observed. For standard $e^+e^- \rightarrow q\bar{q}$ events the rarity r is randomly distributed between 0 and 1 and the exoticness E is expected to be 0 with a variance of 1. For large N_{obs}, which is not the case here, the expected exoticness distribution is a Gaussian, allowing E to be directly interpreted as a "number of sigmas". In the case of small numbers of events, the exoticness probability can be computed analytically using Poisson statistics, as discussed in detail in Ref. [17].

4.3.2   Result of the combination

The rarity distribution is shown in Fig. 11a for the 35 four-jet events. An accumulation of eight events appears with a rarity smaller than 0.05 while standard processes are expected to be essentially uniformly distributed between 0 and 1. When taking this distribution at face value, the probability that it be even more peaked towards small rarity values would be a few 10^{-5}. However, the fact that the observed di-jet mass sum distribution clusters around 105 GeV/c^2
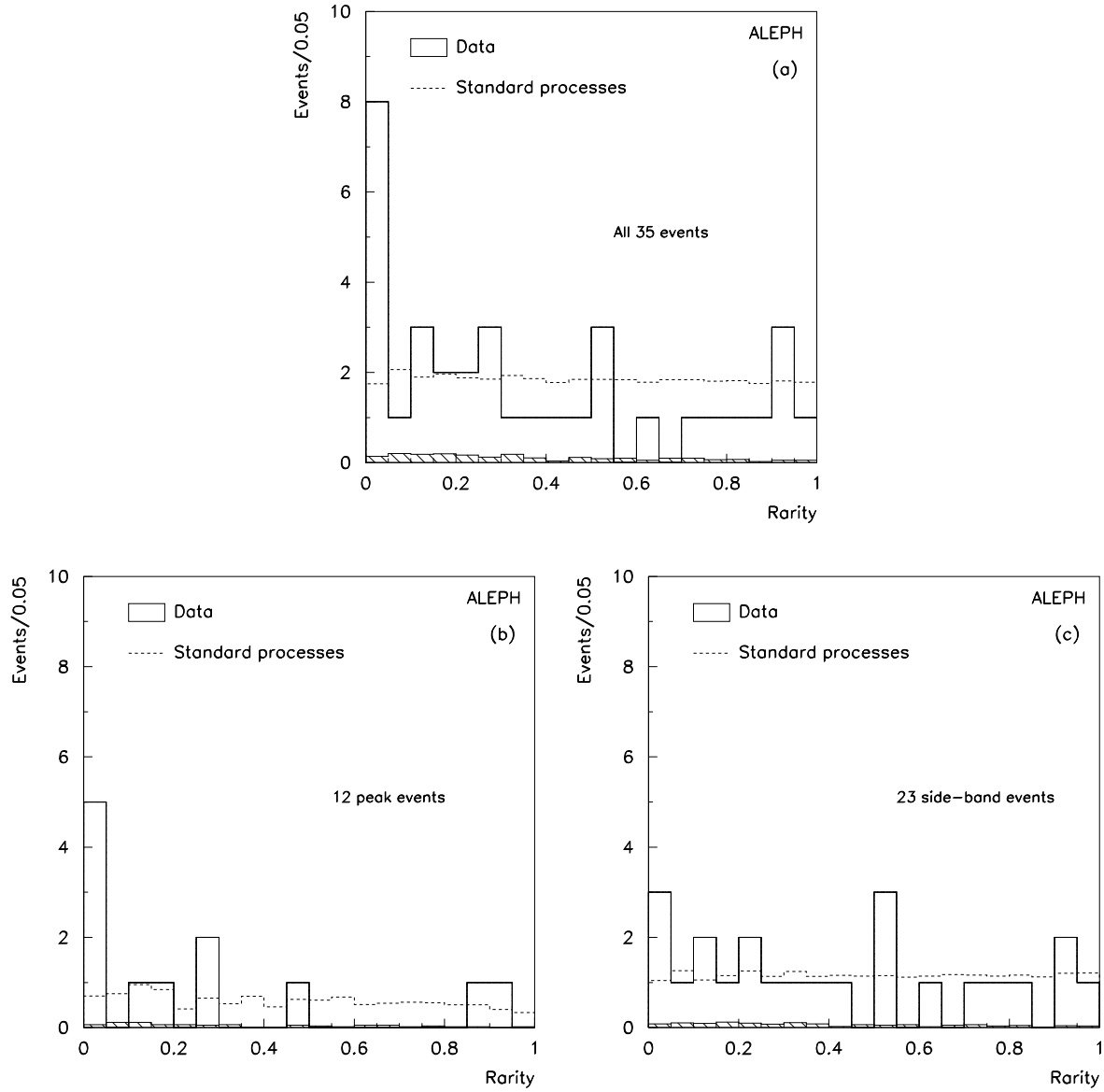
Figure 11: Distributions of the rarity r obtained by combining the QCD matrix element squared and the smallest jet charge for (a) all 35 events; (b) the 12 peak events only; and (c) the 23 sideband events. The standard process prediction, normalized to 35, 12 and 23 events, respectively, is indicated by a dashed line. The hatched histogram represents the contribution of four-fermion processes only (relatively normalized).

has not yet been taken into account, which makes this probability correlated to the ones of Section 3.2 and 3.4.

To address this, the rarity distributions for the peak and the side-band events are shown separately in Fig. 11b and 11c, respectively, and compared with the standard model expectations for events selected in the same di-jet mass sum regions. The second distribution is reasonably compatible with the standard process prediction, with an exoticness probability of $\sim 10\%$. In contrast, the peak events are strongly biased towards small rarity values, while the standard prediction is only slightly affected by the peak event selection. Still ignoring any systematic errors, the probability for these events to be more exotic than observed is 0.02%. This probability breaks down in 1.1% and 1.2% when the parton dynamics and the jet charge are considered separately.

Alternatively, the two-dimensional distributions of the individual rarities *i.e.* the fractions of $e^+e^- \to q\bar{q}$ simulated events *(i)* with a smaller matrix element squared value, r_1; and *(ii)* with a larger smallest jet charge value, r_2; are shown in Fig. 12a and 12b for the peak and the side-band events respectively. The standard processes are uniformly distributed and show essentially no correlation between the two variables. In the data, five of the peak events are found with low values of r_1 and r_2 (see Fig. 12a) where exotic four-quark production would be expected to show up, while less than half an event (out of 12) is expected in this region from standard processes. The above 0.02% probability is mostly due to this clustering at low rarities. In contrast, only one of the 23 side-band events (responsible for the 10% probability) is observed in this region (see Fig. 12b).
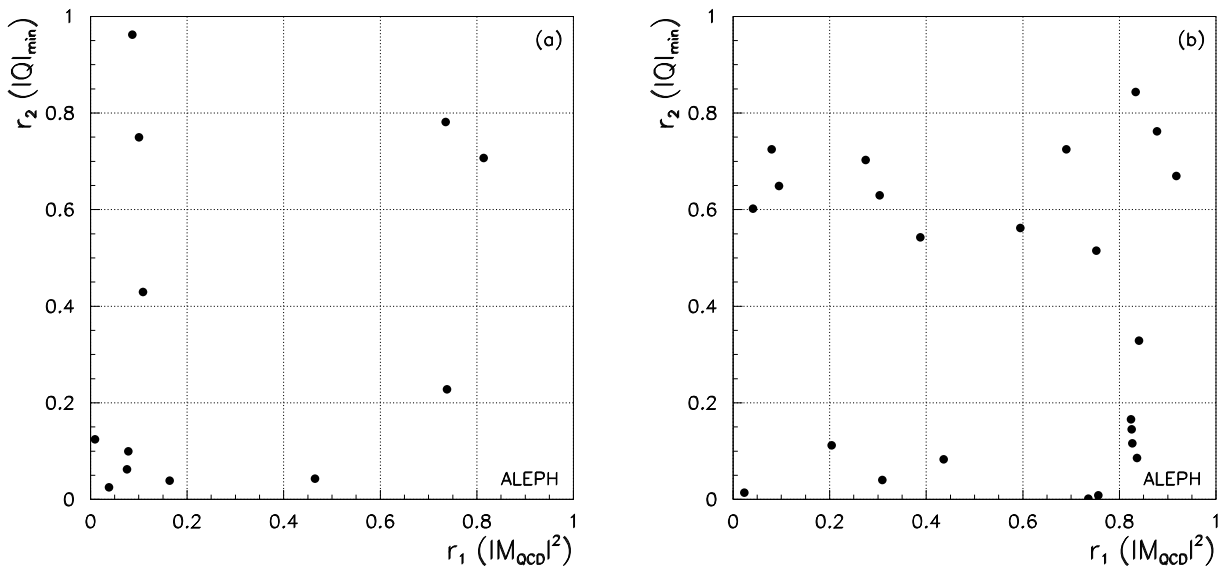

Figure 12: Distributions of the individual rarities (see text) related to the QCD matrix element squared (r_1) and the smallest jet charge (r_2), as seen in the data (a) for the peak and (b) for the side-band events.

19

4.3.3 Systematic studies

To estimate the systematic effects due to the method or to simulation imperfections, the same procedure was applied to the control samples *(ii)* and *(iii)* of Section 3.3.2. As expected from the original individual distributions displayed in Fig. 8 and 10, the resulting probabilities are high (18% and 26% for the 1994 and the 1995 samples, respectively). The corresponding rarity distributions are shown in Fig. 13.
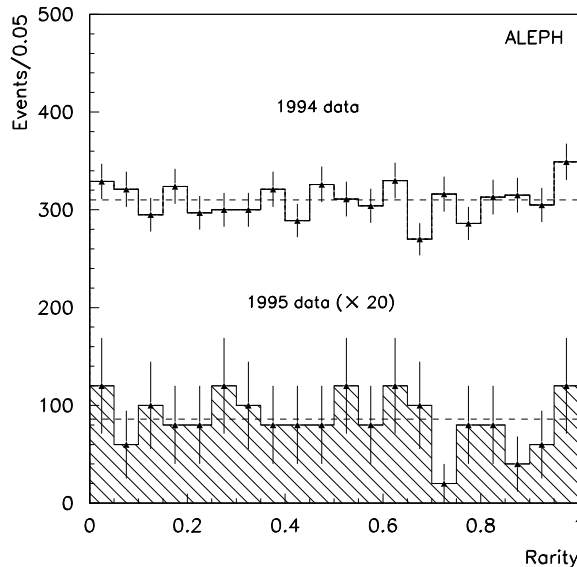

Figure 13: Rarity distribution (see text) for the 1994 (empty histogram) and 1995 (hatched histogram) control samples. The dashed lines are the normalized QCD predictions from JETSET.

Since these control probabilities, although reasonably large, seem to be consistently smaller than 50%, this might be an indication of a slight systematic bias in the simulated samples. The smallest probability, obtained with the combined rarity distribution of the 1994 control sample, is equivalent to a 1σ effect and is interpreted as a systematic bias. To take this bias into account, a correction to the exoticness is applied with two constants a and b such that the mean value and the variance of $\sqrt{N_{94}} \times [a + b \log r]$ of the 1994 sample be 0 and 1 respectively [17]. By doing so, the probability of this sample is driven back to the ideal 50% value. When applying the same correction to the high energy data, the peak event probability is corrected for possible systematic effects and becomes 0.03%.

To be even more conservative, the correction of systematic effects could be evaluated from the 23 side-band events, despite the very low statistics. With correction factors determined from these side-bands as explained above so that the rarity distribution probability becomes 50% instead of 10%, the probability for the peak events would increase to 0.2%. However, as discussed above, the pair production of heavy particles would lead to a signal in the side-bands: a total of 5.3 events would be expected from this source in the side-bands if the peak events were attributed to such a signal. In this hypothesis, therefore, ascribing the entire discrepancy between the data and the simulation to systematic effects results in overestimating the size of such effects.

5 Pair production hypothesis

Since, as shown in the previous section, the 12 peak events show little compatibility with QCD, the possibility may be considered that some of these 12 events originate from the production of a pair of new particles with mass sum 105 GeV/c^2. In this section, more properties of these 12 events are therefore evaluated and compared with the predictions of a few particle pair production hypotheses.

5.1 Production cross section

Under a particle pair production hypothesis, the observed excess of events corresponds to a cross section of 3.1 ± 1.7 pb, assuming the efficiencies evaluated with the $e^+e^- \to hA$ simulated sample (see Section 3.4). This can be compared to the expected production cross section of 0.49 pb for $e^+e^- \to hA$ with $m_h = m_A = 53$ GeV/c^2, corresponding to 1.2 events expected from 5.7 pb^{-1}. Charged Higgs boson production, also suppressed by a β^3 phase space factor, leads to a similar number of expected events.

Production of spin 1/2 particles could better account for the excess of events observed in the data: the point-like cross section is 5.6 pb and it becomes 3.4 pb when multiplied by $\beta = 0.6$, relevant for two particles of mass 53 GeV/c^2. On the other hand, coloured scalar particles would have a production cross section enhanced by a substantial colour factor, and could therefore accomodate the excess too.

5.2 Jet flavours

The most specific property of Higgs boson production followed by hadronic decay is the presence of heavy flavour quarks (b, c, s) in the final states. Both h and A have high branching ratios into $b\bar{b}$ for $\tan\beta \gtrsim 1$ and into $c\bar{c}$ for $\tan\beta \lesssim 1$, and charged Higgs boson hadronic decays lead to $c\bar{s}\bar{c}s$ final states.

Among the 12 peak events, only one has at least two jets that can be tagged as b quark jets with lifetime-tagging algorithms. No lepton with high transverse momentum with respect to its jet [18] is found while 3.2 ± 1.4 would be expected if the 12 events were $b\bar{b}b\bar{b}$ events. No event satisfies a four-b quark final state criterion such as that described in Ref. [19] to be compared to 8.4 ± 1.6 such events expected within 12 $b\bar{b}b\bar{b}$ events. When combined with the cross section and the jet charge information, this result disfavours the $hA \to b\bar{b}b\bar{b}$ hypothesis.

The c and s quark content of these events can be evaluated by searching for secondary vertices from $K_S^0 \to \pi^+\pi^-$ decays [20]. Three K_S^0 are found in agreement with the 2.7 ± 1.4 K_S^0 expected from a normal flavour mixture of standard four-jet events, and slightly lower than the 5.3 ± 1.6 K_S^0 expected from H^+H^- production. Given the large statistical uncertainties, this cannot be used to exclude H^+H^- production. However, the non-observation of $\tau^+\nu_\tau\bar{c}s$ and $\tau^+\nu_\tau\tau^-\bar{\nu}_\tau$ events in chargino searches [21] allows an upper limit to be set on the number of events that can be observed in the $H^+H^- \to c\bar{s}\bar{c}s$ channel. For theoretically favoured values of the $H^+ \to \tau^+\nu_\tau$ branching ratio (i.e. above 50%), this 95% C.L. upper limit is 1.2 events. This, together with the cross section information, disfavours the charged Higgs boson hypothesis.
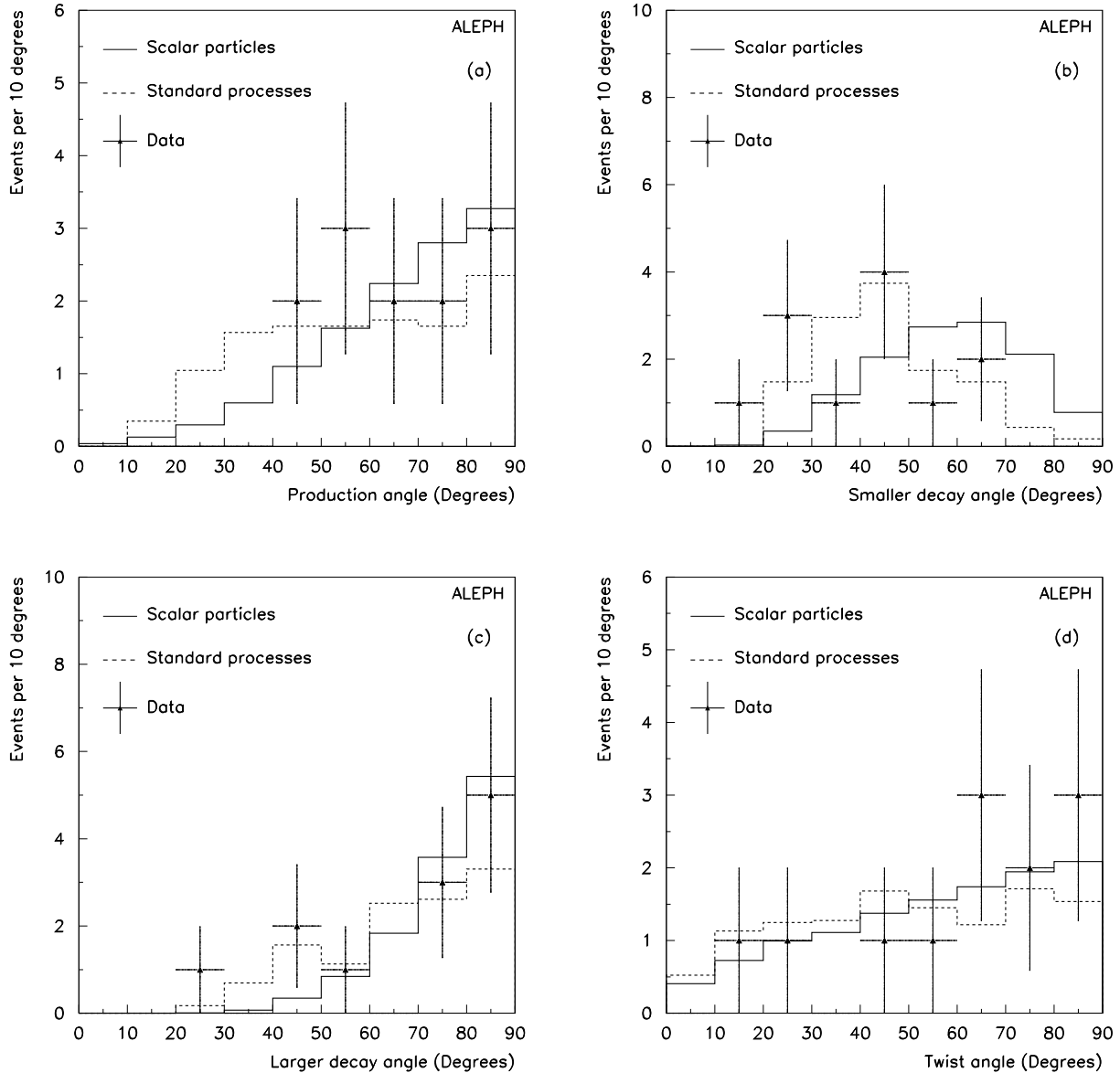
5.3 Angular distributions

Figure 14: Distributions of (a) the production angle, (b) the smaller and (c) the larger decay angle, and (d) the twist angle, for the data (triangles with error bars), the standard processes (dashed histogram) and scalar particle production (solid histogram). The histograms are normalized to 12 events.

To test the scalar particle production hypothesis, the jets are paired to form two particles according to the smallest or the second smallest di-jet mass difference as indicated in Section 3. Four angles, in principle characteristic of the pair production of scalar particles, are then tested: *(i)* the production angle of the two objects, *i.e.* the angle between the direction of their momenta and the beam direction; *(ii)* the two decay angles of the two objects, *i.e.* the angles between the directions of the particle and the jet momenta, measured in the rest frame of the particle;

and *(iii)* the twist angle, *i.e.* the angle between the two decay planes. The distributions of these four angles are shown in Fig. 14 for the 12 peak events, together with the distributions expected in the same di-jet mass sum region from standard processes and from scalar particle production.

Since they have been biased by the selection procedure, none of these angular distributions is very discriminating, in the sense that it would be difficult to make a cut in any of these distributions to reduce the standard process contribution while keeping a high efficiency for the signal. However, the standard processes tend to produce angles smaller, on average, than those expected from scalar particle production. To increase the overall discriminating power, the four angles are combined with the rarity formalism as described in Section 4.3. For each event, the fraction of simulated events from scalar particle production with all four angles larger than that of this event is determined, the corresponding rarity is defined from this fraction as previously. By construction, the rarity is uniformly distributed between 0 and 1 for scalar particle production and peaked at 0 for usual four-jet events.
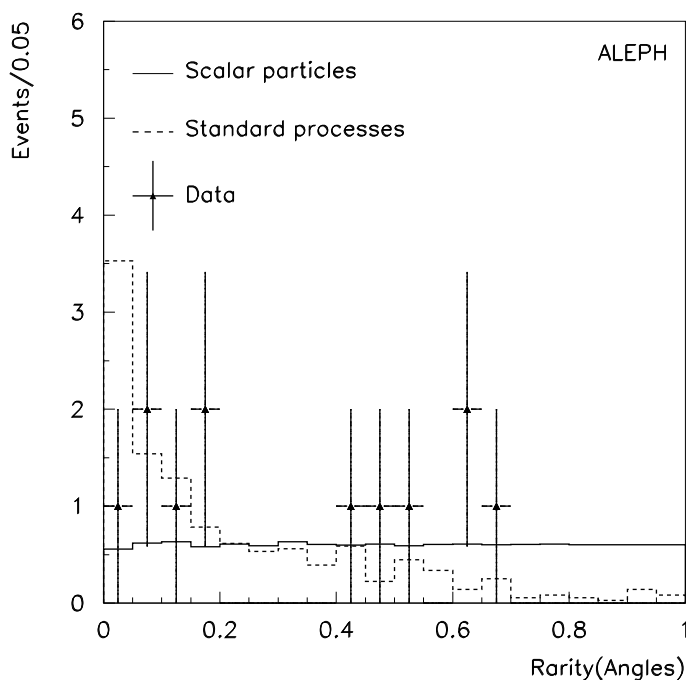

Figure 15: Distribution of the rarity when the four angular distributions (see text) are combined, for the data (triangles with error bars), the standard processes (dashed histogram) and scalar particle production (solid histogram). The histograms are normalized to 12 events.

The distribution of the rarity thus obtained is shown in Fig. 15 for the 12 peak events. The observed distribution does not present as pronounced an enhancement at low rarity values as expected from the standard prediction, but neither is it uniform between 0 and 1 as expected from scalar particle production. The probability that the 12 events come exclusively from scalar particle production, *i.e.* the probability that the rarity distribution be more peaked at zero than observed is only 4.2%, but the probability that these events come exclusively from standard processes is 1.1%. (Due to the correlation between the two decay angles and the QCD

23

matrix element squared, this probability is not independent of that obtained in Section 4.1.) A probability of 50% could be reached for a mixture with one third of standard processes and two thirds of scalar particle production. Due to the small number of events, these fractions have large ($\pm 25\%$) statistical uncertainties.

5.4 Di-jet mass sum and difference

The di-jet mass difference is displayed in Fig. 16 for the 12 peak events together with the predictions from standard processes and from scalar particle production, for the different cases of equal mass scalar particles (such as H^+H^-), of scalar particles with a mass difference of 10 GeV/c^2 (possible with hA) and of coloured equal mass scalar particles (such as squarks).
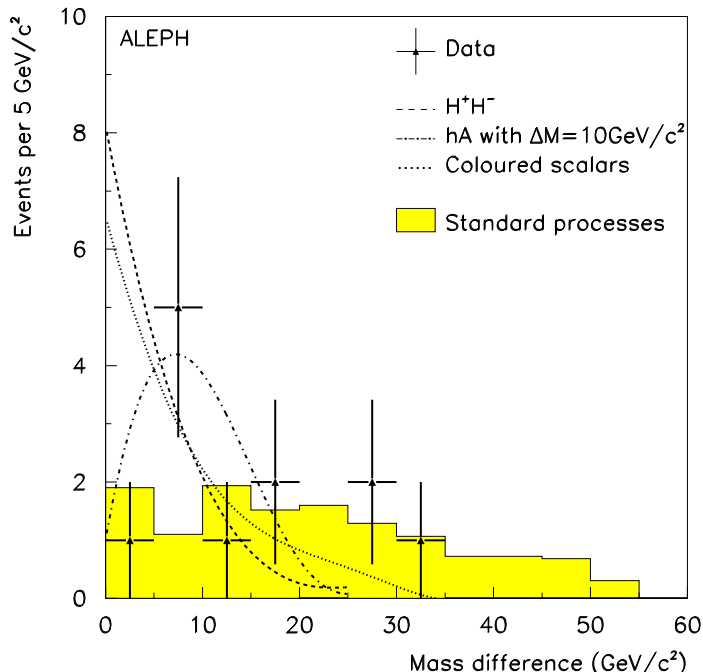

Figure 16: Distribution of the di-jet mass difference for the data (triangles with error bars), the standard processes (shaded histogram) and various scalar particle production processes: colour singlets with equal mass (dashed curve), colour singlets with 10 GeV/c^2 mass difference (dash-dotted curve) and equal-mass coloured scalars (dotted curve). The histograms are normalized to 12 events.

In the latter case, the mass difference resolution is expected to be degraded due to colour connection between the two hemispheres. Non zero-width particles would yield a similar degradation of the resolution. In the $\Delta M = 10$ GeV/c^2 case, the resolution achieved on the mass sum does not differ from the resolution obtained with equal mass particles, but the wrong combination contribution is slightly higher. The di-jet mass difference computed here corresponds to the jet pairing with either the smallest or the second smallest mass difference as defined in Section 3.4, which explains the difference between Fig. 16 and Fig. 2b. The fact that the proportions of events selected with the first and the second smallest mass difference

24

are different in the data compared with the standard processes clearly affects Fig. 16, but has very little effect on the other quantities studied.

The compatibility of the di-jet mass difference distribution with the various hypotheses can be quantified as above with the rarity formalism. In this respect, the probabilities that the 12 events originate exclusively from particle pair production are 0.4%, 20% and 12% for equal-mass colour singlets, 10 GeV/c^2 mass difference colour singlets and equal mass coloured particles, respectively. The probability that these events come solely from standard processes is at the 20% level, and the fractions of standard processes needed to reach a 50% probability are 70%, 25% and 30% in each of the three cases, with even larger errors than those obtained from the angular distributions.

The di-jet mass sum values of the 12 events are listed in Table 7 at the end of this Section. The RMS of the distribution is 2.1 GeV/c^2, slightly larger than what is expected from colour singlet scalar production (1.6 GeV/c^2), and slightly smaller than what is expected from coloured particles (3.0 GeV/c^2). This cannot be used to discriminate between the various pair production hypotheses and standard four-jet production.

5.5   Electric charge

Finally, it is checked whether the 12 peak events are compatible with the pair production of electrically charged particles. An observable directly related to the electric charge of this hypothetical particle is given by the charge separation $\Delta Q = |Q_1 + Q_2 - Q_3 - Q_4|$ between the two jet pairings defined according to the mass difference as in Section 3.4, denoted here 1-2 and 3-4 for convenience, where Q_i is the charge of jet i determined as explained in Section 4.2. A large electric charge would translate into a large value of $\langle \Delta Q \rangle$ while a neutral particle, yielding a low $\langle \Delta Q \rangle$ value, could not be disentangled from the standard processes. The mean value and RMS of the charge separation expected from standard four-jet events and from various pair-produced (neutral and charged) particle decays are listed in Table 6.

The distribution of ΔQ is shown in Fig. 17 for the 12 peak events, together with the standard process prediction and the expectation from different charged particle decay hypotheses. The mean value of ΔQ for the peak events is 0.64 ± 0.09 to be compared to the standard model expectation of 0.38 ± 0.01, and to the predictions from other possible final states (see also Table 6). The probability that the charge separation distribution be more or as biased towards high values is 1.5%. This result is robust against changes in the jet charge definition (momentum vs rapidity weighted jet charge) and in jet algorithm (JADE vs Durham), and is found not to be due to peculiar charged particle multiplicity and rapidity distributions inside the jets. Finally, as can be inferred from the first two lines of Table 6, this is almost uncorrelated with large $|Q|_{\min}$ values since q$\bar{\text{q}}$gg events (with small $|Q|_{\min}$) and u$\bar{\text{u}}$u$\bar{\text{u}}$ events (with large $|Q|_{\min}$) lead to almost the same value of $\langle \Delta Q \rangle$.

The simulation of the charge separation can be systematically checked by comparing the predicted ΔQ distribution with those observed in the two four-jet control samples collected at the Z peak (see Fig. 18a and 18b). No inadequacies of the simulation and no detector imperfections can be seen in these distributions. The two-jet event sample collected at high

Table 6: Mean and RMS values of the charge separation distribution for several four-parton final states. The first two lines are for standard four-jet events, for a normal flavour mixture of four-jet events and for uūuū events only. The five last lines concern particle pair productions, with electric charge 0, 0, 1, 1 and 4/3, and subsequent decays into bb̄, gg, cs̄, ud̄ and uu.

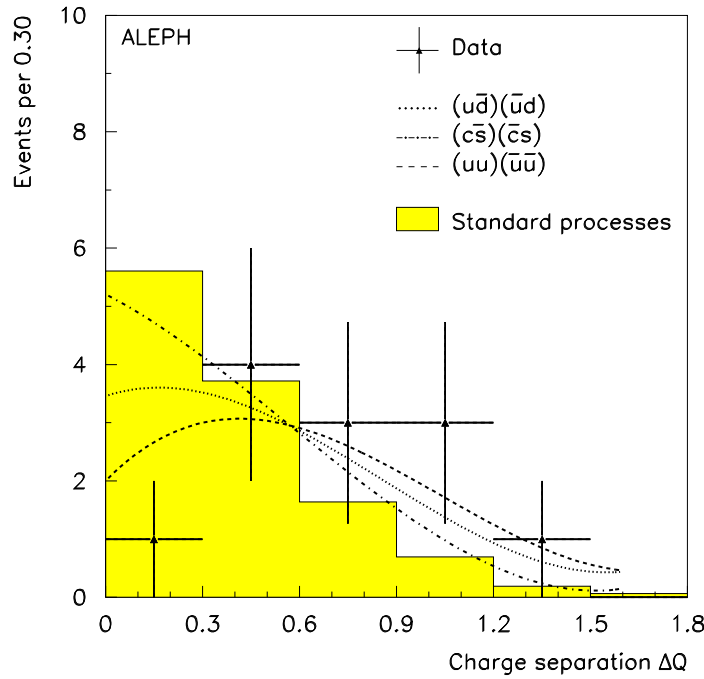| Final state	Mean	RMS
Standard qq̄gg	0.38	0.31
Standard uūuū	0.43	0.33
(bb̄) (bb̄)	0.30	0.24
(gg) (gg)	0.39	0.27
(cs̄) (c̄s)	0.49	0.36
(ud̄) (ūd)	0.57	0.42
(uu) (ūū)	0.64	0.42

Figure 17: Distribution of the charge separation ΔQ for the 12 peak events (triangle with error bars), and as predicted from standard processes (shaded histogram). The predictions of particle pair production with subsequent decays into ud̄ūd (dotted curve) cs̄c̄s (dash-dotted curve) and uuūū (dashed curve) are also indicated.
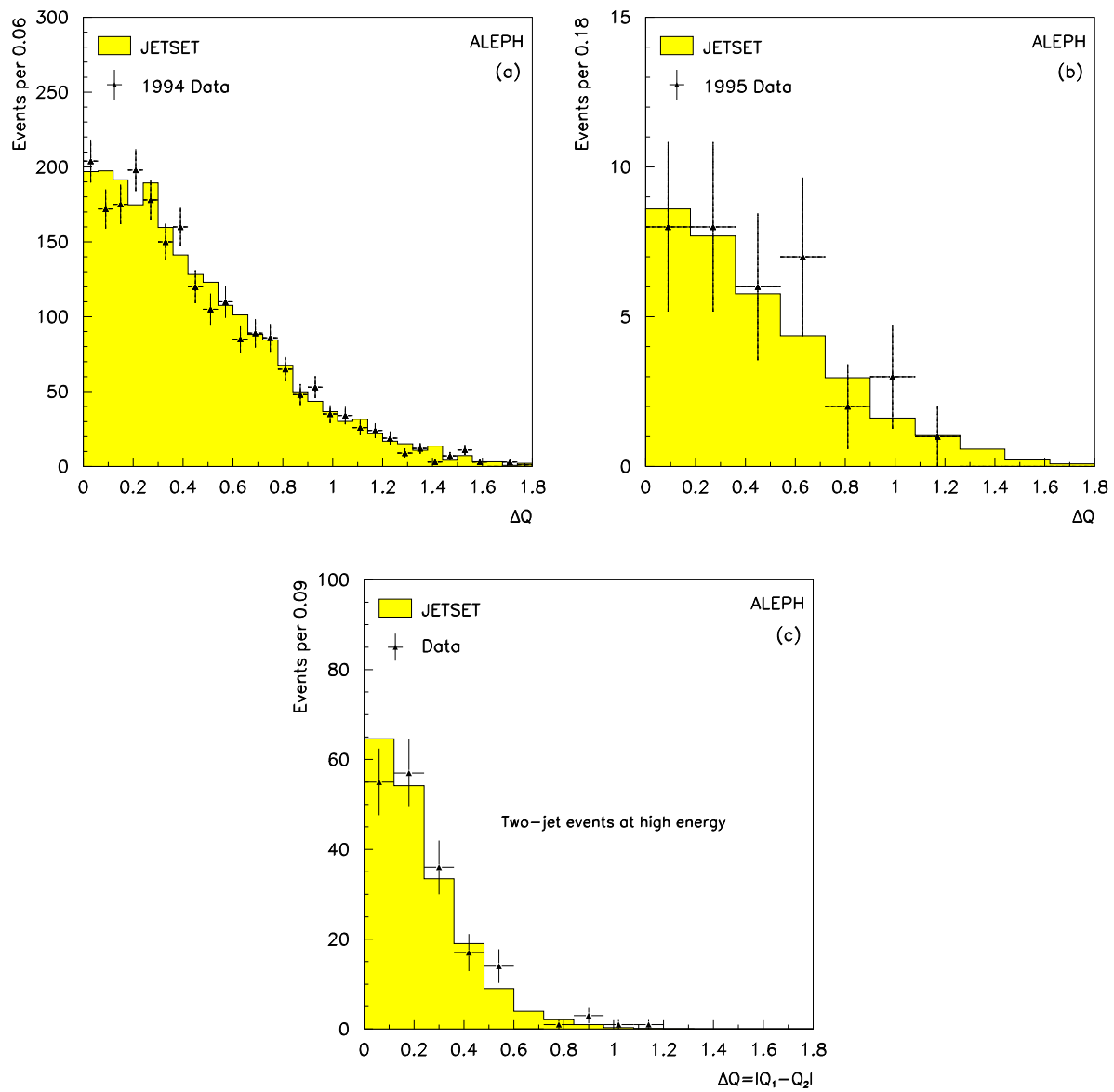
26

Figure 18: Distribution of the charge separation obtained with the (a) 1994 and (b) 1995 four-jet control samples, and (c) with the two-jet sample collected at high energy. The shaded histograms represent the QCD prediction from JETSET.

energy at the same time, and therefore with exactly the same detector configuration, as the four-jet event sample is also in agreement with the expectation (Fig. 18c).

However, nuclear interactions in the detector could have occurred systematically for the peak events, with the effect of adding protons to some of the jets, therefore artificially increasing their charge, and subsequently the charge separation between jet pairings, with two side effects: (i) this would increase the total event charge, while it is measured to be 0.05 ± 0.13 for the 12 peak events, compatible with the standard prediction of 0.04 ± 0.01; and (ii) this would produce an asymmetric individual jet charge distribution biased towards positive values. This distribution, displayed in Fig. 19, is actually symmetric with respect to zero, although slightly broader than the expected distribution from standard four-jet events. For comparison, the distribution expected from events with four u quarks in the final state is also displayed in the same figure.
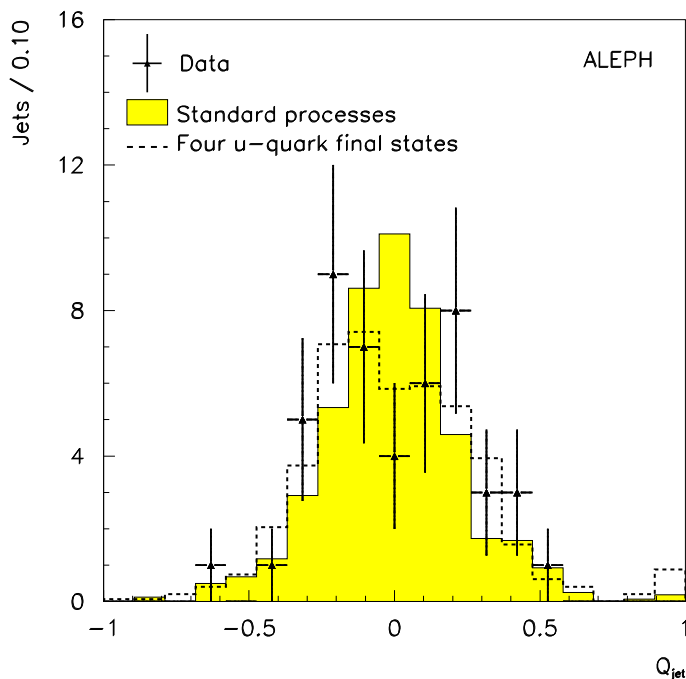

Figure 19: Jet charge distribution (four entries per event) for the 12 peak events (triangles with error bars), for a normal mixture of standard four-jet events (shaded histogram) and for $u\bar{u}u\bar{u}$ events (dashed histogram). The histograms are normalized to 12 events.

To summarize, given the limited discrimination of the variables examined in this Section and the small number of events, it is not possible to distinguish among the various pair production hypotheses. Nevertheless some properties are better constrained by the data than others. The mass sum is about 105 GeV/c^2 and the production cross section is 3.1 ± 1.7 pb. The branching ratio into final states with b quarks is not dominant. From the mass difference distribution, the production of equal-mass, zero-width, color singlets is not favoured. Finally, the production of a pair of electrically neutral particles is also disfavoured.

Table 7: For each event: centre-of-mass energy (in GeV), di-jet mass sum and di-jet mass difference (in GeV/c^2); log of the QCD matrix element squared $|M_{QCD}|^2$ and smallest jet charge $|Q|_{min}$, with the corresponding rarities r_1, r_2 and r; and charge separation ΔQ. The first nine events are selected with the smallest di-jet mass difference, the last three with the second smallest di-jet mass difference.

$\sqrt{s}$	ΣM	ΔM	$\log_{10}|M_{QCD}|^2$	r_1	$|Q|_{min}$	r_2	r	ΔQ
130	103.7	16.5	2.27	0.107	0.05	0.430	0.191	0.33
130	108.4	12.7	2.13	0.035	0.18	0.024	0.005	1.08
130	105.2	10.0	3.02	0.734	0.09	0.227	0.476	0.40
130	107.5	6.8	2.71	0.464	0.15	0.049	0.112	1.22
130	102.1	8.6	3.14	0.818	0.02	0.705	0.902	0.63
136	102.9	17.6	2.22	0.073	0.12	0.094	0.036	0.32
136	102.2	8.5	2.29	0.109	0.02	0.746	0.280	0.97
136	105.3	30.2	2.21	0.071	0.14	0.069	0.023	0.93
136	107.8	0.5	2.37	0.164	0.17	0.036	0.031	0.61
130	106.0	25.7	2.25	0.083	0.01	0.968	0.278	0.16
136	105.2	8.3	1.93	0.001	0.11	0.122	0.005	0.64
136	104.7	29.0	3.02	0.735	0.01	0.781	0.899	0.39

6   Summary

The data collected by the ALEPH detector in November 1995 at centre-of-mass energies of 130 and 136 GeV, corresponding to a total integrated luminosity of 5.7 pb^{-1}, have been analyzed to study the four-jet final state and to search for hadronic decays of pair-produced heavy particles.

The distribution of the sum of the di-jet masses, for the jet pairing with the smallest mass difference, of 16 selected events shows an unexpected accumulation of nine events in a mass interval corresponding to $\pm 2\sigma$ of the detector resolution. The significance of this accumulation is reinforced by three additional events when the jet pairing with the second smallest mass difference is considered instead. The distributions of the QCD matrix element squared, the jet charges and the charge separation of these 12 events show little compatibility with those predicted by standard processes.

Many systematic effects related to the detector and to the analysis method have been taken into account in quantifying the compatibility of each single distribution with the observations. The single probabilities are not combined because a truly meaningful combination should also include other contributions that are difficult to quantify such as *(i)* the contribution of other variables that were studied during this analysis but are not presented because they were considered not to be discriminant; and *(ii)* the fact that many searches for different final states were performed, thus increasing the probability that one among them shows experimental observations that have little compatibility with predictions.

Higher statistics are therefore needed to decide whether these low probabilities are due to a conspiracy of statistical fluctuations or point to some kind of new physics and, in this case, to establish a coherent scenario for it. Additional data are expected to be collected during the year 1996. Meanwhile the purpose of this paper has been to present all the available information.

Acknowledgements

References

[1] D. Decamp et al. (ALEPH Coll.), *Nucl. Instrum. Methods* **A 294** (1990) 121.

[2] D. Buskulic et al. (ALEPH Coll.), *Nucl. Instrum. Methods* **A 360** (1995) 481.

[3] D. Buskulic et al. (ALEPH Coll.), *Phys. Lett.* **B313** (1993) 535.

[4] P. Janot, *"The HZHA generator"* in *"Physics at LEP2"*, Eds. G. Altarelli, T. Sjöstrand and F. Zwirner, CERN 96-01 (1996), Vol. 2, p. 309.

[5] T. Sjöstrand, *"The PYTHIA 5.7 and JETSET 7.4 Manual"*, LU-TP.95/20 and CERN-TH.7112/93.

[6] Y. Dokshitzer, *J. Phys.* **G17** (1991), 1441.

[7] W. Bartel et al. (JADE Coll.), *Z. Phys.* **C33** (1986) 23;
S. Bethke et al. (JADE Coll.), *Phys. Lett.* **B213** (1988) 235.

[8] D. Buskulic et al. (ALEPH Coll.), *"Studies of QCD in $e^+e^- \to$ hadrons at centre-of-mass energies of 130 and 136 GeV "*, submitted to *Phys. Lett.* **B**.

[9] J. Hilgart, R. Kleiss and F. Le Diberder, *Comput. Phys. Commun.* **75** (1993) 191.

[10] D. Buskulic et al. (ALEPH Coll.), *Z. Phys.* **C66** (1995) 3.

[11] F. Le Diberder, *"Study of the e^+e^- annihilation process into four leptons"*, PhD Thesis, LAL 88-21 (1988).

[12] R.K. Ellis, D.A. Ross and A.E. Terrano, *Phys. Rev. Lett.* **45** (1980) 1225; and *Nucl. Phys.* **B178** (1981) 421.
See also: T. Sjöstrand et al. , *"QCD generators"* in *Z Physics at LEP I*, CERN 89-08, Vol. 3 (1989), Eds. G. Altarelli, R. Kleiss and C. Verzegnassi.

[13] D. Buskulic et al. (ALEPH Coll.), *"Determination of* $\sin\theta_W^{eff}$ *Using Jet Charge Measurements in Hadronic Z Decays"*, CERN PPE/96-09 (1996), submitted to *Z. Phys.* **C**.

[14] K. Abe et al. (VENUS Coll.), *Phys. Rev. Lett.* **66** (1991) 280;
D. Decamp et al. (ALEPH Coll.), *Phys. Lett.* **B284** (1992) 151;
P. Abreu et al. (DELPHI Coll.), *Z. Phys.* **C59** (1993) 357.

[15] D. Buskulic et al. (ALEPH Coll.), *"Quark and Gluon Jet Properties in Symmetric Three-Jet Events"*, CERN PPE/95-184 (1995).

[16] D. Buskulic et al. (ALEPH Coll.), *Phys. Lett.* **B356** (1995) 409.

[17] F. Le Diberder, *"Rarity and Exoticness"*, Mark II/SLC Note 245 (1989).

[18] D. Buskulic et al. (ALEPH Coll.), *Nucl. Instrum. Methods* **A 346** (1994) 461.

[19] D. Buskulic et al. (ALEPH Coll.), *"Search for the* $hA \rightarrow b\bar{b}b\bar{b}$ *final state in two Higgs doublet models"*, Contribution to the Int. Europhysics Conference on High Energy Physics, Brussels, Belgium, July 27 - August 2, 1995, Ref. EPS0415;
See also: S. Simion, *"Search for neutral Higgs bosons in two Higgs doublet models with the ALEPH detector at LEP"*, PhD Thesis, LAL 95-14 (1995).

[20] D. Buskulic et al. (ALEPH Coll.), *Z. Phys.* **C64** (1994) 219.

[21] D. Buskulic et al. (ALEPH Coll.), *"Search for supersymmetric particles in* e^+e^- *collisions of centre-of-mass energies of 130 and 136 GeV"*, CERN PPE/96-10 (1996), submitted to *Phys. Lett.* **B**.